Chapter 1.
REVIEW OF THE FIELD

1.1. Introduction

High energy particle accelerators are now the primary means of discovering the basic building blocks of matter and understanding the forces between them. In order to minimize the cost of building these machines, superconducting magnets are used in essentially all present day high energy proton and heavy ion colliders. The cost of superconducting magnets is typically in the range of 20-30% of the total cost of building such machines. The circulating particle beam goes through these magnets a large number of times (over hundreds of millions). The luminosity performance and life time of the beam in these machines depends significantly on the field quality in these magnets. Therefore, even a small error in the magnetic field shape may create a large cumulative effect in the beam trajectory to throw the particles out of the magnet aperture. The superconducting accelerator magnets must, therefore, be designed and constructed so that these errors are small. In this thesis the research and development work will be described which has resulted in a significant improvements in the field quality of the superconducting magnets for the Relativistic Heavy Ion Collider (RHIC) [140]. The design and the field quality improvements in the prototype of the main collider dipole magnet for the Superconducting Super Collider (SSC) [143] will also be presented.

RHIC will accelerate and collide two counter rotating beams of heavy ions up to 100 GeV/u and protons up to 250 GeV. It is expected [112] that RHIC will create a hot, dense quark-gluon plasma and the conditions which, according to the Big Bang theory, existed in the early universe.

1.2. Physics Potentials and Goals of RHIC

The physics potentials and goals of RHIC have been extensively discussed in a number of places [11,112,125,136,153,173]. The following summary is based on these and some other reports.

Two high energy heavy ion beams will collide at RHIC. This will create nuclear matter whose temperature and density will be much higher than ever produced in a controlled environment. The baryon density will be over ten times that in normal matter. Baryons are strongly interacting particles which are made of 2 quarks (in mesons) or 3 quarks (in hadrons). According to present theories, the total number of quarks is six, namely, up (u), down (d), strange (s), charm (c), bottom (b) and top (t). The interaction between the quarks is carried by gluons and the theory describing these interactions [145] is called Quantum Chromodynamics (QCD). According to some calculations based on QCD, a quark-gluon plasma (QGP) should be observed at RHIC. In a quark-gluon plasma, the usually confined interacting quarks and gluons move around freely. Such conditions are predicted when the baryon density is about ten times that in the normal conditions or when the temperature is about 2×10^{12} degree kelvin ($\sim$ 150 MeV).

The protons and neutrons (of which stable nuclei are made) are dominantly made of up and down quarks; contributions from gluons and quark-anti-quark pairs from the fermi sea are also present. However, according to the theory strange quarks are much easier to create in a quark-gluon plasma and the particles/resonances based on them are expected to be made in abundance. In normal conditions the interaction between quarks is strong and attractive. Moreover, the attractive force grows rapidly in strength as the separation between the quarks increases. This leads to the confinement theories according to which it is impossible to observe a quark in a free state. However, in extreme thermodynamic conditions of temperature and density, a phase transition is predicted. In this new thermodynamic phase of the quark gluon plasma (QGP), the conditions will be such that the attractive forces which bind quark-anti-quark pairs in mesons and three quarks in hadrons will be overcome. This will lead to a deconfined state of high-energy-density matter (plasma) where the quarks will move freely. The lifetime of this phase should be long enough ($\sim 10^{-22}$ sec) to be observed in RHIC experiments. The primary goals of RHIC experiments [112] will be to confirm these predictions and to study the properties of this new state of matter. A detailed investigation of this state, the formation of it and the other states to follow from it [153] will also be interesting. A phase diagram [112] of nuclear matter is

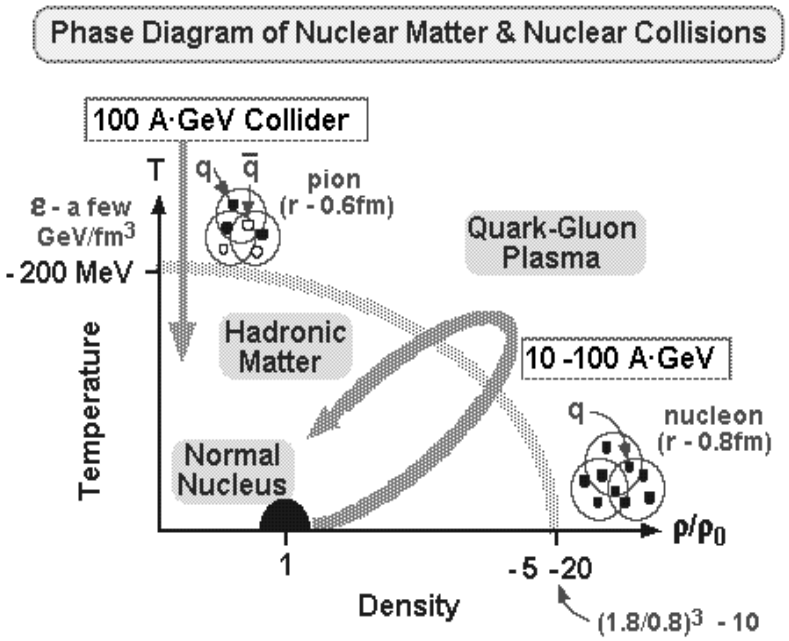

Figure 1.2.1: Phase Diagram

shown in Fig. 1.2.1, where temperature is plotted vs. net baryon density for an extended volume of nuclear matter in thermal equilibrium.

According to QCD theories, the lowest energy state is not the vacuum with no particles (and hence no interaction) in it. The lowest energy state is actually the vacuum filled with quark-anti-quark pairs (fermi sea). The relative ratio (mix) of densities between various type of quark-anti-quark pairs is determined by QCD. A preference of one type of mix over another is attributed to the spontaneous breaking of chiral symmetry in the normal phase. However, in the new thermodynamic phase of a quark gluon plasma chiral symmetry is restored with no preference given to one mix of quark-anti-quark pairs over another. Moreover, according to theories, a large number of otherwise rare strange quarks and strange anti-quarks will be generated. These quarks will eventually decay but the process is slow (on a nuclear time scale) and the secondary particles generated from them will signal the existence of such a situation to RHIC detectors.

It is expected that a quark-gluon plasma will be created in RHIC. This state has not been created before in a laboratory environment and perhaps does not exist any where in the world today. According to theories this state existed for only 5-10 microseconds after the Big Bang and was crucial to determining the structure of the universe as we see today. This state may give a new insight to our understanding of the world and may even create phenomena which are not expected from the present theories. The use of large heavy ions in colliders allows this state to persist for a relatively long time since the lifetime is expected to be at least (or even much greater than) the radius of the nuclei divided by the velocity of light. In this respect RHIC (Relativistic Heavy Ion Collider) is in a unique situation in which the beam (heavy ions including gold with a radius of 7 fermi), the machine and the detectors are all designed with this new phase in mind.

A number of detectors and experiments are designed to study the various aspects of the quark-gluon plasma and other physics expected from RHIC. In addition to observing the strongly interacting particles, the detectors will also use the leptons and photons to obtain a signal from the quark gluon plasma. RHIC will also be studying spin physics based on 250 GeV on 250 GeV collisions between polarized protons. There are plans for installing four detectors in four interaction regions. These detectors are STAR (Solenoidal Tracker At RHIC) [146], PHENIX [134], PHOBOS [112] and BRAHMS (Broad Range Hadron Measuring Spectrometer) [9].

1.3. Overview of RHIC Machine

A major nuclear physics facility, the Relativistic Heavy Ion Collider (RHIC), is being built at the Brookhaven National Laboratory. A brief description and its present status is described in recent papers [84,85]. A complete description is given in the RHIC design manual [140]. The following description of RHIC is primarily based on these reports.

RHIC will accelerate heavy ions (for example gold) to a nominal maximum energy of 100 GeV/u and protons to 250 GeV. A brief list of the major parameters [140] of the RHIC machine is given in Table 1.3.1. RHIC has two rings with the orbit of the two counter rotating beams switching alternatively between the inner and outer rings at the six beam crossing points. The circumference of the machine will be 3.834 km and it has six interaction regions for experiments where the beam can be collided head-on or at a small angle. Each interaction region has a free space of ± 9 meter on the either side of the crossing point for detectors before a magnet of the RHIC lattice appears. The design storage time for gold ions at the maximum energy is 10 hours. The design luminosity for gold ions at the top energy is $2 \times 10^{26} cm^{-2} sec^{-1}$. The luminosity will be lower at lower energies and the storage time may well be decreased.

The injection energy of beams to RHIC will be in the range of 10.8 GeV/u (for gold ions) to 28.3 GeV (for protons). In order for this beam to reach RHIC a series of beam transfer lines and existing accelerators will be used. The heavy ions will come from the existing Tandem Van de Graff which uses a pulsed sputter ion source. The gold beam leaving the Tandem Van de Graff facility will have a charge state of +14 and a kinetic energy of 1 MeV/u. This beam will be transported through a long ($\sim$550 m) transfer line and injected into the Booster. The Booster (circumference 201.781 m) will accelerate this beam to 72 MeV/u energy after which the beam will pass through a stripping target for removing more electrons from the nuclei. The gold ions having a charge state of +77 will be selected for further transmission. This beam will be injected into the Alternating Gradient Synchrotron (AGS, circumference 807.125 m) through a beam transport line. The AGS will accelerate this beam to an energy of 10.8 GeV/u. The extracted beam from the AGS will go through another target and the nuclei will be completely stripped of all electrons to reach the final charge state of +79. The final beam transport line from AGS to RHIC will split into two lines to inject beams into the two RHIC rings. The protons will come from the existing linear accelerator (LINAC) facility. A 200 Mev polarized (low intensity) or unpolarized (high intensity) H^- beam will be injected into the Booster. The stripper

Table 1.3.1: Major Parameters for RHIC

Kinetic Energy, Injection-Top (each beam), Au	10.8-100 GeV/u
protons	28.3-250 GeV
Luminosity, Au-Au at 100 GeV/u & 10 h av.	$\sim 2\times10^{26}$ cm^{-2} sec^{-1}
No. of bunches/ring	60
No. of Au-ions/bunch	1×10^{9}
Storage time for Au at $\gamma > 30$	~10 hours
Diamond length	180 mm rms
Circumference, 4-3/4 C_{AGS}	3833.845 m
Beam separation in arcs	900 mm
Number of crossing points	6
Free space at crossing point	$\pm$9 m
Beta at crossing, horizontal/vertical	10 m
low-beta insertion	1 m
Crossing angle, nominal (maximum)	0 ($<$ 1.7) mrad
Betatron tune, horizontal/vertical	28.19/29.18
Transition Energy, γ_T	22.89
Magnetic Rigidity, Bρ at injection	97.5 T·m
Magnetic Rigidity, Bρ at top energy	839.5 T·m
Bending radius, arc dipole	242.781 m
No. of dipoles (192/ring + 12 common)	396
No. of quadrupoles (276 arc + 216 insertion)	492
Dipole field at 100 GeV/u, Au	3.46 T
Arc dipole length, effective	9.45 m
Arc Dipole length, physical	9.73 m
Dipole current	5.1 kA
Arc quadrupole gradient	~71 T/m
Arc quadrupole length, effective	1.11 m
Coil i.d. arc magnets	80 mm
Beam tube i.d.	69 mm
Operating temperature, Helium refrigerant	$<$ 4.6 K
Refrigeration capacity at 4 K	24.8 kW
Cooldown time, entire system	~7 days
Vacuum, warm beam tube sections	$\sim 7\times10^{-10}$ mbar
Filling time (each ring)	$<$ 1 min
Injection kicker strength (95 nsec)	~0.18 T·m
Beam stored energy	~200 kJ
rf voltage, h=360	600 kV
rf voltage, h=2520	6 MV
Acceleration time	~ 1 min

inside the Booster (to facilitate charge exchange injection) will convert H^- ions to protons which will then be accelerated to an energy of 1.5 GeV. From this point onward the beam will follow the same path as described above for gold. The AGS will accelerate protons to an energy of 28.3 GeV which will then be injected into two RHIC rings.

As per the present design, each RHIC ring will have 60 bunches injected in 20 cycles with three bunches from the AGS in each cycle. It will take about 1 minute to fill the rings. The separation between bunches will be 64 m (or 213 nsec in time). The arc magnet power supply will be ramped at a rate of 70 A/sec from a current of $\sim$0.57 kA (0.4 T) at injection to a maximum current of $\sim$ 5.1 kA (3.46 T) at the top energy. Therefore, it takes about one minute to accelerate the beam from injection energy to top energy. At the time of injection the radio-frequency (rf) system, which operates at $\sim$28.2 MHz will have a voltage of approximately 200 kV. During acceleration this voltage will be adiabaticlly raised to $\sim$ 300 kV. The storage system uses a different rf system, one that operates at 197 MHz frequency.

The RHIC lattice is designed to be identical for the two counter rotating beam. It is composed of six circular arcs and six straight sections. The lattice has three super periods with each super period consisted of inner arc, insertion, outer arc and insertion. Each arc consists of 11 FODO cells (22 dipoles, 11 focusing and 11 defocusing quadrupoles) and each insertion has twelve dipoles and 18 quadrupoles. The nominal horizontal and vertical operating tune of the machine are ν_H=28.19 and ν_V=29.18. The transition energy (γ_T) is 22.89. During injection and acceleration the size of the beam at the crossing point will be large (β^*=10). The beam size will be gradually reduced (β^*=1) for higher luminosity. At injection the performance of the machine will be dominated by the field errors in the 80 mm aperture arc dipole magnets and at storage the luminosity performance of RHIC will be dominated by the field errors in the 130 mm aperture insertion quadrupole magnets.

1.4. Superconducting Magnets

In this section a brief description of the cosine theta superconducting magnets is given. A more complete description can be found elsewhere [86,128,144,175,177,179]. Type *II* superconductors, which allow penetration of magnetic field lines, are used in all superconducting magnets. They can retain their superconducting state up to a field of $\sim$20 tesla and are being currently used in designing magnets in the range of 3 to 15 tesla. Type *I* superconductors, which were discovered first and which completely exclude field lines, lose superconductivity at a much lower field of 0.18 tesla or below and therefore are not suitable for such applications. Despite the promising prospects of high temperature superconductors [93] they are not yet suitable for accelerator magnets.

In superconducting magnets which are mostly intended for operation above 3 tesla maximum field, the field shape is primarily determined by the superconducting coils. Superferric magnets are a hybrid version of superconducting and iron dominated room temperature magnets. In superferric magnets though, superconducting coils are used but the iron plays an important role in shaping the field. The research work described here is limited to superconducting magnets.

The two main design goals for superconducting magnets are to obtain (a) a good quench performance (a quench implies the loss of superconductivity in the cable) and (b) a good field quality. After an overall introduction to the magnet geometry, the superconducting cable, the cryogenic system, the magnetic design, the mechanical design, the magnet construction and the magnet measurements will be briefly described.

1.4.1. Introduction to the Magnet Geometry

Superconducting accelerator magnets are basically long cylindrical magnets whose cross section is mostly uniform along the length except at the two ends. The cross section of the 80 mm aperture RHIC arc dipole magnet inside the cryostat is shown in Fig. 1.4.1. The overall size of superconducting magnets is usually much larger then the aperture required for the particle beam. As compared to the 80 mm coil inner diameter and 69 mm beam tube inner diameter, the outside diameter of the RHIC cryostat is 610 mm. Similarly, in the SSC main dipole magnet design, for a coil aperture of 50 mm, the cryostat outside diameter was 660 mm.

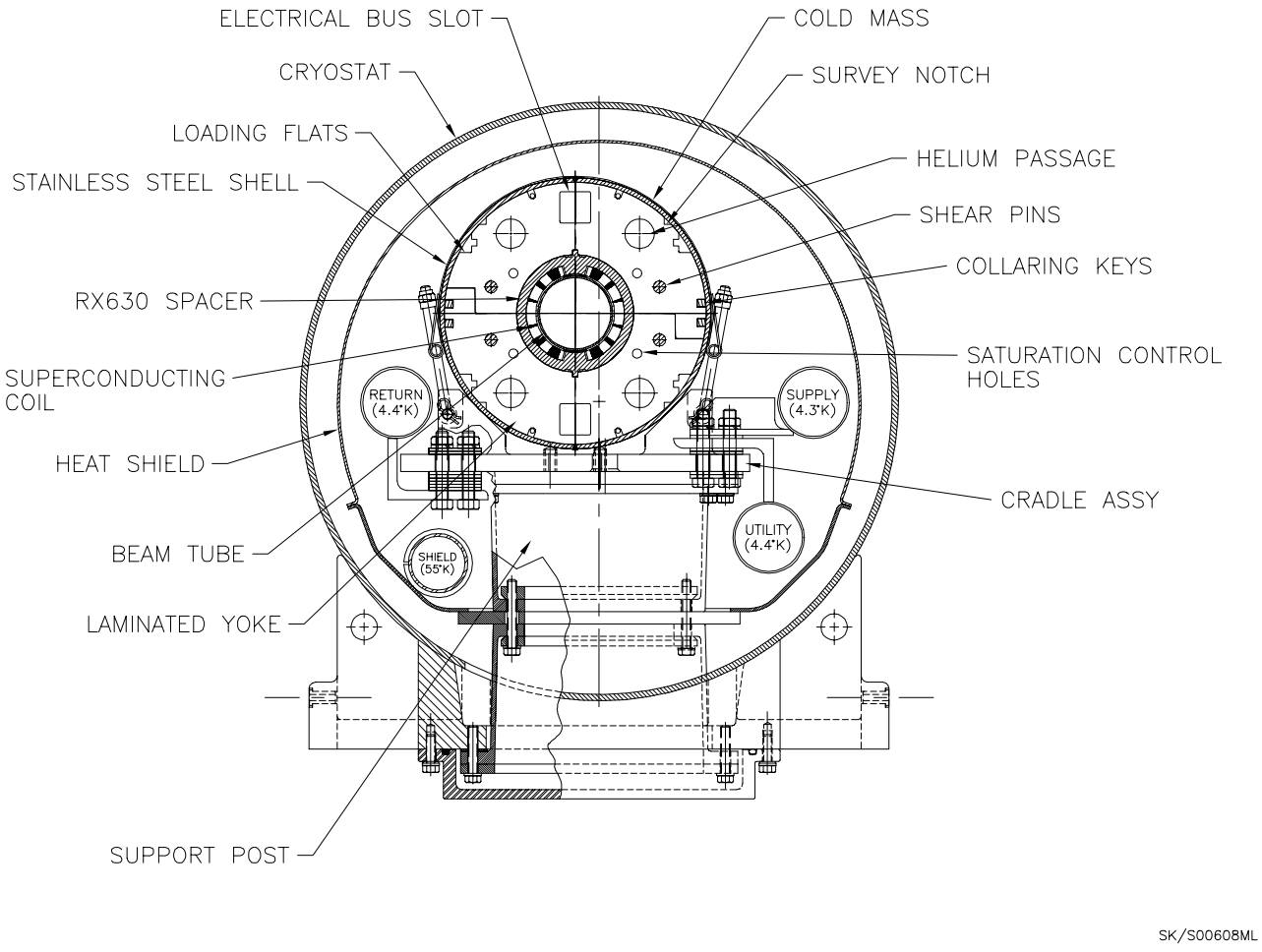

Figure 1.4.1: A cross section of the 80 mm aperture RHIC arc dipole magnet with the important magnetic, mechanical and cryogenic system components marked. The cold mass is asymmetrically located inside the cryostat. The cross section shown here is at the axial center.

The superconducting coils are made of Nb-Ti superconductor configured in a *"Rutherford Type"* [154,176] cable. The coils are kept below a temperature of 4.65 kelvin. The cryogenic system is designed to minimize the heat leak to room temperature outside the cryostat. The coils are kept under compression to minimize conductor motion under Lorentz forces when the magnet is energized. In RHIC magnets the space between the superconducting coils and the yoke is filled with RX630 phenolic spacers and in SSC magnets with stainless steel collars. The purpose of the yoke is to provide magnetic shielding and additional field in the magnet aperture. The yoke has several features (see Fig. 1.4.1) to serve a variety of purposes. These features include (a) loading flats to provide compression on the coil through a heavy press (b) holes for helium flow, saturation control and yoke pins (c) cutouts for electrical bus work, collaring keys, tabs which align the RX630 spacers to define the coil pole location and survey notches for aligning the magnet in the cryostat. A stainless steel shell, which also provides radial pressure, is put outside the yoke for helium containment.

The part of the magnet assembly described above (superconducting coils, iron yoke and stainless steel) is called the "coldmass" which remains below 4.65 degree kelvin in RHIC and SSC designs. The coldmass is put inside the cryostat which is a vacuum vessel. A number of components between the coldmass and the cryostat are required for structural and thermal purposes.

1.4.2. Superconducting Cable

In most magnet designs the superconducting wire is made of NbTi filaments embedded in a copper matrix. NbTi has good mechanical properties (ductility) but is generally limited to producing $\sim$7.5 tesla at 4.5 kelvin and $\sim$10.5 tesla at 1.8 kelvin. A higher field can be reached with the more expensive Nb_3Sn superconductor. However, Nb_3Sn does not have similarly good mechanical properties and therefore coil manufacturing becomes much more complicated. The titanium in NbTi alloy is generally about 46% by weight. The measured critical current density (the current density at which the wire looses its superconducting properties) as a function of applied field at 4.2 K is shown in Fig. 1.4.2 (courtesy A. Ghosh) for the NbTI wire used in RHIC corrector magnets. A similar $B-J$ performance is obtained in the superconducting cable used in the other types of RHIC magnets. In addition to the superconductor, the cable contains copper to provide stability against quench and for

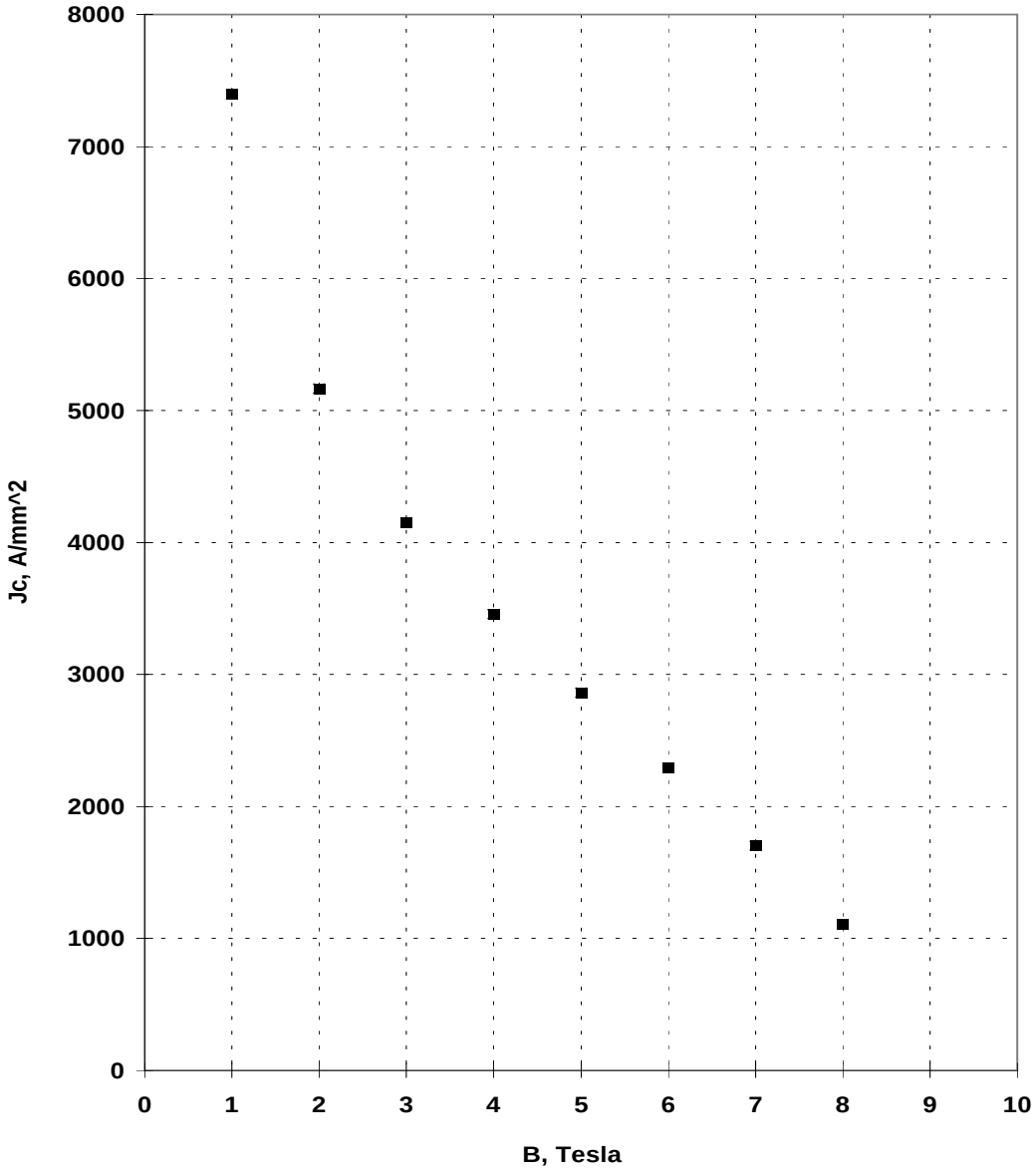

Figure 1.4.2: The measured (courtesy A. Ghosh) critical current density (J_c) at 4.2 K in the superconductor of the wire used in the RHIC corrector magnets as a function of applied field (B).

heat conduction. The amount of copper in the cable is usually more than the amount of superconductor. The superconducting cable, used in RHIC magnets, has a copper to superconductor ratio (by volume) of 3.0 in corrector magnets, of 2.5 in trim quadrupole and sextupole magnets, of 2.2 in the 80 mm and 100 mm aperture magnets and 1.8 in the 130 mm aperture and 180 mm aperture insertion magnets. The cable used in the inner layer of the SSC dipole had a copper to superconductor ratio of 1.3 and the one used in the outer layer had a copper to superconductor ratio of 1.8. The filament size in the superconducting wire used in the RHIC and SSC dipole magnet design is 6 μm except for the wire used in the RHIC corrector, sextupole and trim quadrupole magnets where it is 10 μm. There are about 3500 filaments in each wire of the RHIC dipole cable. The wire (strand) diameter is about 0.65 mm. The parameter list of the cable used in RHIC dipole magnet is given in Table 1.4.1.

Table 1.4.1: Design specifications of the superconducting cable for the 80 mm aperture RHIC arc dipole and quadrupole magnets.

Cable parameters	Value
Filament diameter	6.0 μm
Filament spacing	>1.0 μm
Number of filaments per wire	3510 $\pm$ 20
Copper to Superconductor Ratio	(2.25$\pm$0.1):1
Strand (wire) diameter	0.648$\pm$0.003 mm
No. of strands in cable	30
Critical current in wire at 5 T, 4.2 K	264 A
Critical current in cable at 5 T, 4.2 K	7524 A
Cable width	9.73 $\pm$ 0.03 mm
Cable mid-thickness	1.166$\pm$0.006 mm
Cable keystone angle	1.2$\pm$0.1 degree
Cable lay pitch	74 $\pm$5 mm

"Rutherford" cable is used in most large scale production of accelerator magnets. This type of cable is wide and flat and is made of a number of wires (strands) twisted together in a spiral shape. The cable is asymmetrically compressed across the flat side with one edge being thinner than the other. This provides a "keystone" angle in the cable which helps the coils to conform to a circular geometry with each turn lying approximately on a radius. In a fully keystoned cable, the ratio of thickness of the two edges of the cable is the same as that between the coil inner radius and outer radius. The cable is electrically insulated to deal with the high voltage (over 1 kV) that is created during a quench when one turn is in the superconducting phase and the other in the normal. The RHIC design uses all-Kapton (Kapton is a registered trademark of Dupont Corporation) insulation which has good electrical break down, cryogenic and stability in ionizing radiation properties and has good dimensional tolerance. Another type of insulation used on superconducting cables is fiberglass tape impregnated with B-stage epoxy.

The superconducting cable produced for the RHIC magnet program is the result of significant R&D and a close collaboration with industry. The standard deviation in the variation in the cable thickness and other mechanical dimensions has been generally kept to about the 5 μm level. This has been crucial to providing good field quality and proper compression on the coils in the magnet. Moreover, the variation in the critical current density is also kept to about 2% to minimize the variation in the field harmonics associated with superconductor effects.

1.4.3. Cryogenic System

Cooling is provided by supercritical helium. A small radial gap between the beam tube and the superconducting coil provides a space for helium flow which partly cools the coil and removes the heat deposited during machine operation or instability in the magnet. The major portion of the heat removal and helium flow takes place in the four helium holes in the yoke. In order to reduce the heat load on the cryogenic system, the design of the coldmass and cryostat is optimized to minimize heat leak. To deal with a large thermal gradient between the low temperature in the superconducting coils and room temperature outside the cryostat, either one or two staged thermal shields are used where the heat is intercepted and removed. In the SSC dipole design two stage heat removal was planned (a) at 20 kelvin by gaseous helium and (b) at 80 kelvin by liquid nitrogen. In the RHIC

dipole design, heat leakage is removed at 55 kelvin. Since the radiation heat leak loss goes as the difference between the fourth power of the two temperatures, only a small difference is expected between the two and one shield cases. A blanket of thermal insulation is placed just inside the vacuum vessel wall and between and interior to the shields.

The coldmass is put inside the vessel on a few support posts. The location of the support posts is chosen to reduce sagging of the coldmass. To minimize the heat leak through them, they are made as long as possible and to accommodate that larger length without increasing the cryostat outer diameter, the coldmass is positioned above the center of the cryostat (see Fig. 1.4.1). In both RHIC and SSC magnets the cryostat is made of low carbon magnetic steel which reduces the exterior field. However, a systematic offset between the vertical center of the cryostat and the center of the coldmass creates a skew quadrupole harmonic in the dipole at high field.

1.4.4. Mechanical Design

Good quench performance of the superconducting magnets is closely related to a good mechanical design which minimizes the motion of the superconducting wires. The design must be structurally sound to deal with the Lorentz forces when the magnet is energized, the thermal forces during cool-down and the mechanical forces during transportation of the magnet.

A large magnetic field in superconducting magnets generates a large Lorentz forces on the superconducting coils which may cause a small amount of conductor motion. This conductor motion generates heat which may start a quench in the magnet. The direction of the Lorentz forces in the cross section of the magnet is such that compression of the coil from the coil pole to the coil midplane is by the azimuthal component and compression outward is by the radial component. To deal with this situation, the coils are pre-compressed with a large mechanical compressive force which counters the Lorentz forces and thus minimizes conductor movement. In the SSC magnets, this compression on the coil is provided by stainless steel collars and in RHIC magnets by the yoke itself. In these designs, a significant part of the compression applied at room temperature is lost when the magnet is brought to a lower temperature. This is because of a difference in the coefficients of thermal expansion of superconducting coils, stainless steel and the yoke iron. Therefore, in order to assure an adequate compression when the magnet is cold, a much higher (a factor of two to three)

compression is applied at room temperature. There are some alternate design concepts which have been tested in some magnets, where this loss of compression is avoided [41,127].

Finally a stainless steel shell is welded on the yoke outer diameter to contain the helium. This also provides a radial pressure on the coil-yoke assembly and in the RHIC-type design the radial component of the Lorentz forces are finally transmitted to it. To deal with the outward axial component of the Lorentz forces, the ends are restrained and sometimes even compressed (loaded) axially. A detailed description of the mechanical design and analysis of the SSC magnets can be found elsewhere [44].

1.4.5. Magnetic Design

The main goal of the magnetic design is to optimize the geometry of the coil and iron shape to produce a highly uniform field. In addition, it is beneficial to minimize the maximum field on the conductor (peak field) and to maximize the transfer function (tesla per ampere) to obtain a high quench field (computed from cable short sample measurements). The design must also fulfill all mechanical and cryogenic requirements and a magnet based on this design should be as simple as possible to manufacture.

The coils are made of a number of turns of superconducting cable which are grouped in several current blocks. A cosine theta current distribution produces an ideal dipole field. Copper wedges are placed between the blocks of turns to approximate the cosine theta current distribution. In designs which use partially keystoned cables, the wedges also serve an important mechanical purpose in providing a proper arc shape to the current blocks in the circular coil geometry. The size of the current blocks and the copper wedges are parameters used to minimize the field harmonics and to maximize the quench field.

The iron yoke provides magnetic shielding. In addition, the magnetized yoke gives an extra contribution to the central field which in most RHIC magnets is $\sim$50% of the coil field. However, at high field, the magnetization in the iron yoke is not proportional to the current in the coils, so the yoke geometry must be carefully designed to maintain a good field quality at all fields.

The coil end design is complicated. The cable must be bent carefully to bring it from one side of the coil to the other side. Spacers are inserted between the blocks of turns in the end not only to minimize the peak field and field harmonics but also for the mechanical purpose of reducing the strain on the cable. In most RHIC magnet designs the ends are

enclosed by the iron yoke laminations but in SSC and in most other magnet designs the iron laminations are replaced by stainless steel laminations to minimize the peak field in the ends.

The field errors in magnets are described in terms of field harmonics (see next section Eq. (1.5.17)) which are also referred to as multipoles. The are generally divided in the following three categories based on their sources :

1. Geometric multipoles
2. Persistent current multipoles
3. Saturation multipoles

The geometric multipoles are related to the magnet geometry. An error (or a departure) from the ideal geometry would create harmonics other than those desired. The persistent current multipoles are related to the persistent current in the superconductors. As the field in magnet is changed, the persistent (shielding) currents are induced in a direction to oppose the changing field [144]. Unlike in normal conductors, these currents persist for a long time in superconductors and contribute significantly to the field errors at low fields where their relative contribution is high. The saturation multipoles are related to the saturation magnetization of iron at high field. A non-uniform field and hence a non-uniform (as a function of azimuth) relative contribution of the iron distorts the field shape and field errors are thereby introduced.

1.4.6. Magnet Construction

The construction of the superconducting magnets is a long and complex process which requires a high level of engineering and quality control to assure consistently good quality in large scale magnet production [6]. The magnet manufacturing tooling must itself be carefully designed to realize the computed field quality and quench performance. Some of the major steps of the manufacturing process are briefly described here in the case of RHIC arc dipole magnets.

The superconducting cable and the copper wedges are insulated with Kapton layers. The magnet coils are wound on a precision convex surface with a winding machine feeding the cable continuously. The copper wedges in the coil cross section and the wedge tips in the coil ends are periodically inserted as required by the optimized design. The Kapton tape, wound around the cable, is coated on one side with a dry adhesive which is activated (cured)

by heat at a temperature of about 130 C while under compression. The coils are cured in a curing fixture (mold) and the temperature and curing pressure described above may contain several curing cycles with different combinations of curing temperature and curing pressure. Once cooled, the coil is firmly fixed in the shape determined by the dimensions of the curing mold.

The coils are installed in the iron yoke together with the RX630 phenolic spacers and other parts. The following is the sequence of the steps required in this operation: (a) the laminations for the lower yoke half are stacked (b) the RX630 spacers are put in place (c) the lower coil is installed (d) the beam tube is inserted (e) the upper coil, pre-assembled with the RX630 insulator, is put in place and (f) the laminations for the upper yoke half are stacked on this assembly. The coil is compressed with a press applying pressure on the yoke collar at the loading flats. The keys are inserted to retain this compression. The stainless steel shell is welded with the required sagitta (axial curvature of the magnet) in the coldmass. The stainless steel end plates are welded and coil end force is applied before the electrical installation is completed. Then the coldmass is placed inside the cryostat on the support posts. All cryogenic piping and heat shields are also installed.

1.4.7. Magnet Measurements

Apart from a variety of mechanical and electrical measurements at the various stages of magnet construction, the two measurements which define the final quality of magnets for machine operation are (a) the quench performance and (b) the field harmonics. For these measurements the magnets must be tested at cryogenic temperatures. It is, however, expensive and time consuming to test each and every magnet cold (in the superconducting phase). Therefore, in the RHIC magnet program only a part of the magnets are tested cold before they are installed in the tunnel [170]. The selection of the magnets chosen for cold testing is carefully made to minimize the risk of not testing all magnets cold. The required maximum operating current for RHIC is about 5 kA and the design margin over the machine requirements for most magnets for the computed quench current is over 30%. The measured performance of the magnets tested cold show that most magnets require only a few (2-5) quenches to reach the computed quench current [170].

Warm magnetic measurements are performed on all magnets. At room temperature, the current in the cable is carried by the copper intermixed with the superconductor. There is an

expected systematic difference between warm and cold harmonics because of (a) a change in the magnet geometry due to thermal contraction during cool-down (b) the persistent current effects in the superconductor and (c) the saturation effects due to the non-linear properties of the iron yoke. Based on those magnets that are tested both warm and cold, a good warm-to-cold correlation in the field harmonics has been obtained [170]. This correlation is used to estimate the field quality in those magnets that are not tested cold.

The magnetic measurements are carried out with an array of windings having a certain radius [175], mounted on a rotating cylinder which intercept the field in the magnet aperture. The geometry of these coils is chosen so that the Fourier analysis of the voltage induced in the various windings determine the field harmonics. The accuracy of the measurements depends on the accuracy of the measuring coil geometry, the electronic signal measurement and the analysis of the measured signal.

In the long curved RHIC magnets, the complete measurements are made in 10 steps with a meter long measuring coil system which is referred to as a mole [49]. In addition, the integral of the field along the axis is also measured with a long stationary coil. For a more accurate measurement of the field strength at a point an NMR (Nuclear Magnetic Resonance) probe is also used.

The measured field quality in 80 mm aperture RHIC arc dipoles is shown in Table 1.4.2 and Table 1.4.3. Measuring the field harmonics accurately and managing it in a large number of magnets (1740 are required for RHIC) is a quite complex task.

The "Mean" of the distribution for the harmonic b_n (which is also sometimes referred to as the systematic value of b_n) in N magnets is defined as follows :

$$< b_n >= \frac{1}{N}\sum_{k=1}^{N}(b_n)_k, \tag{1.4.1}$$

where $(b_n)_k$ is the value of harmonic b_n in the k^{th} magnet. The "SIGMA" (σ), also the RMS (Root Mean Square) deviation from the "Mean" b_n, is defined as follows :

$$\sigma\,(b_n) = \sqrt{\frac{1}{N}\sum_{k=1}^{N}\left[(b_n)_k - < b_n >\right]^2}. \tag{1.4.2}$$

The primary purpose of the harmonic measurements is to verify that the machine requirements needed for beam stability and design beam life time in RHIC are satisfied. In addition, the field harmonics are also used as a tool to detect possible manufacturing defects in the magnets or a drift in the mechanical dimensions of the components used in

the manufacturing process. Since the harmonics are the analysis of the field created by the geometry of the coil and yoke, they are a reflection of magnet geometry. The accuracy of the magnetic measurements is sufficient to find a 100μm or less error in most of the critical components used in manufacturing the magnets.

Table 1.4.2: The measured integral transfer function (ITF) in tesla·m/kA, body transfer function (SSTF) in tesla/kA and normal field harmonics (b_n, defined elsewhere) at 25 mm reference radius in the 9.45 m long 80 mm aperture RHIC arc dipole magnets (data courtesy Jain and Wanderer). The current at which measurements are made and the number of magnets (shown in parenthesis) used in arriving at the statistics are shown here. The 30 A measurements are made when the magnet is warm (room temperature), in the non-superconducting state and the current is carried by the copper in the cable. $< b_n >$ is the mean and $\sigma(b_n)$ is the standard deviation of harmonic b_n in the number of magnets measured.

	$< b_n > \pm\sigma(b_n)$	$< b_n > \pm\sigma(b_n)$	$< b_n > \pm\sigma(b_n)$	$< b_n > \pm\sigma(b_n)$
	30A(296)	660A(63)	1450A(61)	5000A(62)
ITF	6.6545± 0.0021	6.6698± 0.0027	6.6769± 0.0021	6.4180± 0.0024
SSTF	0.7042± 0.00021	0.7078± 0.0003	0.7080± 0.00028	0.6798± 0.00034
b_1	0.25±0.37	0.08±0.28	0.04±0.27	0.10±0.28
b_2	3.54±1.74	-0.17±2.22	2.18±1.77	0.83±1.76
b_3	-0.03±0.10	0.00±0.08	0.00±0.08	0.01±0.08
b_4	0.22±0.44	-0.33±0.57	-0.15±0.58	0.15±0.59
b_5	0.01±0.03	0.00±0.03	0.00±0.03	-0.03±0.04
b_6	0.12±0.11	-0.13±0.13	-0.02±0.14	1.19±0.14
b_7	0.00±0.01	-0.01±0.01	-0.01±0.01	-0.01±0.01
b_8	0.09±0.11	0.14±0.12	0.13±0.12	0.12±0.12
b_9	0.00±0.01	0.02±0.02	0.02±0.02	0.02±0.02
b_{10}	-0.53±0.02	-0.58±0.02	-0.56±0.02	-0.58±0.02

Table 1.4.3: The measured a_n (skew harmonics) at 25 mm reference radius in the 9.45 m long 80 mm aperture RHIC arc dipole magnets (data courtesy Jain and Wanderer). The current at which the measurements are made and the number of magnets (shown in parenthesis) used in arriving at the statistics are shown here. The 30 A measurements are made when the magnet is warm (room temperature), non-superconducting and the current is carried by the copper in the cable. $< a_n >$ is the mean and $\sigma(a_n)$ is the standard deviation a_n in the number of magnets measured.

	$< a_n > \pm\sigma(a_n)$	$< a_n > \pm\sigma(a_n)$	$< a_n > \pm\sigma(a_n)$	$< a_n > \pm\sigma(a_n)$
	30A(296)	660A(63)	1450A(61)	5000A(62)
a_1	-0.20±1.62	0.28±1.53	0.21±1.52	-1.51±1.51
a_2	-1.11±0.20	-1.03±0.17	-1.03±0.17	-1.07±0.18
a_3	-0.01±0.49	-0.03±0.42	-0.02±0.42	-0.36±0.41
a_4	0.18±0.07	0.21±0.06	0.21±0.06	0.20±0.06
a_5	-0.01±0.17	0.02±0.15	0.01±0.15	-0.06±0.16
a_6	-0.11±0.03	-0.10±0.02	-0.10±0.02	-0.10±0.02
a_7	0.00±0.05	-0.01±0.05	-0.01±0.05	-0.01±0.05
a_8	0.02±0.01	0.02±0.01	0.02±0.01	0.02±0.01
a_9	0.00±0.01	0.04±0.02	0.04±0.02	0.04±0.02
a_{10}	-0.01±0.00	-0.01±0.01	-0.01±0.01	-0.01±0.01

1.5. Magnetic Field Analysis in Accelerator Magnets

In this section an outline of the formalism and theory used in carrying out the field calculations in the superconducting magnets is given. Starting from first principles, basic expressions are developed which are used in designing and describing the magnetic fields in the accelerator magnets.

The uniformity of the magnetic field is very important since it determines the performance of the machine. A typical requirement for the field quality in the accelerator magnets is that the deviation from the ideal shape should be within a few parts in 10^4. The uniformity of the field is expressed in terms of the Fourier harmonic components.

1.5.1. Basic Electromagnetic Field Equations

The calculation of the magnetic field in accelerator magnets is too complex to be done directly by solving Maxwell's equations. However, the most complicated formulae describing the field shape in the magnets are derived primarily from them. In this section, Maxwell's equations and other commonly used expressions of electro-magnetic theory [95,129,150] are briefly described. Although the magnetic field in the accelerator magnets is not static in time, the effects of time variation are by and large negligible in the problems to be addressed during the course of this work. Therefore, most of the detailed analysis is limited to the magneto-static case only.

The four Maxwell's equations are :

$$\nabla \cdot \vec{D} = \rho, \tag{1.5.1a}$$

$$\nabla \cdot \vec{B} = 0, \tag{1.5.1b}$$

$$\nabla \times \vec{E} + \frac{\partial \vec{B}}{\partial t} = 0, \tag{1.5.1c}$$

$$\nabla \times \vec{H} = \vec{J} + \frac{\partial \vec{D}}{\partial t}. \tag{1.5.1d}$$

Here $\vec{H}$ is the magnetic field, $\vec{E}$ is the electric field, $\vec{B}$ is the magnetic induction and $\vec{D}$ is the displacement vector. ρ denotes the charge density and $\vec{J}$ the current density, and these two are related by the following continuity equation,

$$\nabla \cdot \vec{J} + \frac{\partial \rho}{\partial t} = 0. \tag{1.5.2}$$

Furthermore, $\vec{B}$ and $\vec{H}$ are related by the following equations:

$$\frac{\vec{B}}{\mu_o} = \vec{H} + \vec{M}, \tag{1.5.3a}$$

$$\frac{\vec{B}}{\mu\mu_o} = \vec{H}, \tag{1.5.3b}$$

where μ_o is the permeability of the vacuum ($\mu_o = 4\pi \times 10^{-7}$ henry/meter) and μ is the relative permeability of the medium (relative with respect to that of vacuum). Often, μ is simply referred to as the permeability (which is in fact the case in CGS units) and the same convention is followed here unless otherwise explicitly mentioned. $\vec{M}$ denotes the magnetization (or magnetic polarization) of the medium. In free space (vacuum) $\vec{M}$ is 0. In an isotropic medium $\vec{H}$, $\vec{B}$ and $\vec{M}$ are parallel to each other.

Furthermore, $\vec{D}$ and $\vec{E}$ are related by the following equations:

$$\vec{D} = \epsilon_o \vec{E} + \vec{P}, \tag{1.5.4a}$$

$$\vec{D} = \epsilon\epsilon_o \vec{E}, \tag{1.5.4b}$$

where $\vec{P}$ is the electric polarization and ϵ_o is the permittivity in vacuum ($\epsilon_o = 8.854 \times 10^{-12}$ farad/meter). ϵ is the relative permittivity of the medium. In free space (vacuum), the electric polarization is 0.

The constants ϵ_o and μ_o are related through the relation

$$\epsilon_o \mu_o = \frac{1}{c^2},$$

where c is the velocity of light (c=2.998 $\times$ 10^8 m/s). Since $\vec{B}$ has a zero divergence, it may be expressed in term of a magnetic vector potential $\vec{A}$ as

$$\vec{B} = \nabla \times \vec{A}. \tag{1.5.5}$$

The vector potential $\vec{A}$ can be obtained at any point ($\vec{r}$) due to a current density $\vec{J}(\vec{r'})$ with the help of the following integral equation :

$$\vec{A}\,(\vec{r}) = \frac{\mu\mu_o}{4\pi} \int_V \frac{\vec{J}\left(\vec{r'}\right)}{|\vec{r} - \vec{r'}|} dv, \tag{1.5.6}$$

where $\vec{r}$ and $\vec{r'}$ are three dimensional coordinates and dv is the three dimensional volume element.

The components of the field in Eqs. (1.5.5) in Cartesian coordinates are given by

$$B_x = \frac{\partial A_z}{\partial y} - \frac{\partial A_y}{\partial z}, \tag{1.5.7a}$$

$$B_y = \frac{\partial A_x}{\partial z} - \frac{\partial A_z}{\partial x}, \tag{1.5.7b}$$

$$B_z = \frac{\partial A_y}{\partial x} - \frac{\partial A_z}{\partial y}, \tag{1.5.7c}$$

and in cylindrical coordinates by

$$B_r = \frac{1}{r}\left(\frac{\partial A_z}{\partial \theta}\right) - \frac{\partial A_\theta}{\partial z}, \tag{1.5.7d}$$

$$B_\theta = \frac{\partial A_r}{\partial z} - \frac{\partial A_z}{\partial r}, \tag{1.5.7e}$$

$$B_z = \frac{1}{r}\left(\frac{\partial (rA_\theta)}{\partial r} - \frac{\partial A_r}{\partial \theta}\right). \tag{1.5.7f}$$

The research work to be described is restricted to static magnetic fields only and electric fields are not considered. During the accelerating cycle of the machine, the magnetic field does change with time in the superconducting magnets. However, for the problems to be discussed during the course of this work, the change in magnetic field has negligible effect on field quality. Therefore the following two Maxwell's equations for the magnetostatic case are used in developing various formulae

$$\nabla \cdot \vec{B} = 0, \tag{1.5.8a}$$

$$\nabla \times \vec{H} = \vec{J}. \tag{1.5.8b}$$

Ampère's law

$$\oint_S \vec{H} \cdot d\boldsymbol{s} = I, \tag{1.5.9}$$

can be obtained from Eqs. (1.5.8b) by integrating and using Stoke's theorem :

$$\oint_C \vec{V} \cdot d\vec{l} = \int_S \left(\nabla \times \vec{V}\right) \cdot \vec{n} da$$

where $\vec{V}$ is a well behaved vector field, S is an open arbitrary surface, C is the closed curve bounding S, d$\vec{l}$ is a line element of C, and $\vec{n}$ is a vector element normal to S. The right hand side of the equation simply states that I = $\int \vec{J} \cdot \vec{n} da$ is the total current flowing through the area.

Poisson's equation for the vector potential is derived here under the assumptions that $\vec{B} = \mu_0 \mu \vec{H}$, the medium is homogeneous (i.e. μ is constant over a finite space) and isotropic. Using $\vec{B} = \mu_0 \mu \vec{H}$ and $\vec{B} = \nabla \times \vec{A}$ in Eqs. (1.5.8), one obtains :

$$\nabla \times \nabla \times \vec{A} = \mu_0 \mu \vec{J}. \tag{1.5.10}$$

The following identity is used to simplify the above equation :

$$\nabla^2 \vec{A} = \nabla \left(\nabla \cdot \vec{A} \right) - \nabla \times \nabla \times \vec{A}. \tag{1.5.11}$$

In Cartesian coordinates the above Laplacian operator (∇^2) can be applied to a vector $\vec{A}$ whose i^{th} component is $\nabla^2 A_i$. In other coordinate systems Eq. (1.5.11) must be used to determine the expression for $\nabla^2 \vec{A}$. In the cylindrical coordinate system :

$$\nabla^2 \vec{A}_z = \frac{1}{r} \frac{\partial}{\partial r} \left(r \frac{\partial A_z}{\partial r} \right) + \frac{1}{r^2} \frac{\partial^2 A_z}{\partial \theta^2}, \tag{1.5.12}$$

when $A_r = A_\theta = 0$ by symmetry (axial symmetric case).

The choice of $\nabla \cdot \vec{A}$ has thus far has been arbitrary and it is made zero in the Coulomb gauge (in the magnetostatic case). In that case Eq. (1.5.10) leads to Poisson's Equation as

$$\nabla^2 \vec{A} = -\mu_0 \mu \vec{J}. \tag{1.5.13}$$

In the 2-dimensional case, when the direction of current flow is parallel to the z-axis, $J_x = J_y = 0$. This implies that $A_x = A_y = 0$ and $\frac{\partial A_z}{\partial z} = 0$. Therefore, the above expression becomes,

$$\nabla^2 A_z = -\mu_0 \mu J_z, \tag{1.5.14}$$

which in the Cartesian coordinate system gives :

$$\frac{\partial^2 A_z}{\partial x^2} + \frac{\partial^2 A_z}{\partial y^2} = -\mu_0 \mu J_z. \tag{1.5.15}$$

In the case of axial symmetry, the Eq. (1.5.14) in cylindrical coordinates becomes :

$$\frac{1}{r} \frac{\partial}{\partial r} \left(r \frac{\partial A_z}{\partial r} \right) + \frac{1}{r^2} \frac{\partial^2 A_z}{\partial \theta^2} = -\mu_0 \mu J_z, \tag{1.5.16}$$

on using Eq. (1.5.12).

1.5.2. Field Harmonic Definitions

It is useful to describe the magnetic field inside the aperture of accelerator magnets in terms of harmonic coefficients [96,140,144,175]. The discussion will be limited to 2-dimensional analysis, which describes the field in the body (or straight section) of a long magnet. When the magnetic field is evaluated a few aperture diameters away from the two ends of the magnet, the axial component of the field is negligible. The accelerator magnets examined here are those in which the field is consists of one fundamental harmonic which is several orders of magnitude larger (usually 10^4) than any other harmonic present.

The skew (a_n) and the normal (b_n) field harmonics are defined through the following relation :

$$B_y + iB_x = 10^{-4} B_{R_0} \sum_{n=0}^{\infty} [b_n + i\ a_n] [cos\,(n\theta) + i\ sin\,(n\theta)] \left(\frac{r}{R_0}\right)^n , \qquad (1.5.17)$$

where B_x and B_y are the horizontal and vertical components of the magnetic field at (r,θ) and $i = \sqrt{-1}$. R_0 is the normalization radius. The magnets for the Relativistic Heavy Ion Collider (RHIC) have a coil radius ranging from 40 mm to 90 mm. In most of these magnets, the normalization radius is taken to be $\frac{5}{8}$ of the coil radius. The value of the normalization radius is 25 mm for the 80 mm aperture diameter of the RHIC arc dipoles and quadrupoles, 40 mm for the 130 mm aperture of the RHIC insertion quadrupoles, 31 mm for the 100 mm aperture of the RHIC insertion dipoles and 60 mm for the 180 mm aperture RHIC insertion dipoles [140]. B_{R_0} is the magnitude of the field due to the fundamental harmonic at the reference radius on the midplane. In the dipoles, $B_{R_0} = B_0$ (the field at the center of the magnet), in the quadrupoles, $B_{R_0} = G \times R_0$ (G being the field gradient at the center of the magnet), and in general for a $2(m+1)^{th}$ pole magnet,

$$B_{R_0} = \frac{R^m}{m!} \left[\frac{\partial^m B_y}{\partial x^m}\right]_{x=0,y=0} . \qquad (1.5.18)$$

Eq. (1.5.17) can be re-written in several other forms using complex variables. In this section z represents the complex coordinate and $B(z)$ represents the complex field as follows:

$$z = x\ +\ i\ y,$$
$$(x\ +\ i\ y)^n = r^n\,(cos\,[n\theta]\ +\ i\ sin\,[n\theta]),$$
$$B\,(z) = B_y\ +\ i\ B_x,$$
$$c_n = b_n +\ i\ a_n,$$

Thus :

$$B_y + iB_x = 10^{-4} B_{R_0} \sum_{n=0}^{\infty} [b_n + i\ a_n] [x\ +\ i\ y]^n \left(\frac{1}{R_0}\right)^n \tag{1.5.19}$$

$$B(z) = 10^{-4} B_{R_0} \sum_{n=0}^{\infty} c_n \left(\frac{z}{R_0}\right)^n \tag{1.5.20}$$

The harmonics used so far ($a_n,\ b_n,\ c_n$) are all dimensionless coefficients. However, in another representation, the field is expressed in terms of coefficients which carry the units of magnetic field. These are usually distinguished from the harmonics a_n and b_n given in Eq. (1.5.17) by the use of the uppercase alphabet. The two are related as follows:

$$A_{n+1} = 10^{-4} B_{R_0}\ a_n, \tag{1.5.21a}$$

$$B_{n+1} = 10^{-4} B_{R_0}\ b_n, \tag{1.5.21b}$$

$$C_{n+1} = 10^{-4} B_{R_0}\ c_n. \tag{1.5.21c}$$

Using these, Eq. (1.5.20) can be written as :

$$B(z) = \sum_{n=1}^{\infty} C_n \left(\frac{z}{R_0}\right)^{n-1}. \tag{1.5.22}$$

In this case the summation begins from $n = 1$ instead of $n = 0$. Sometimes C_n is also written as $C(n)$.

The definition for the field harmonics used so far is the one which is more common in U.S. laboratories. The European laboratories (such as CERN and HERA) use a slightly different definition [179]. The two are related as follows :

$$(a_{n+1})_{Europe} = -10^{-4}\ (a_n)_{US}$$

$$(b_{n+1})_{Europe} = 10^{-4}\ (b_n)_{US}$$

Yet another representation of field harmonic is used in beam dynamics calculations where the particle trajectory is studied in the machine [25]. For this purpose, the field is expressed in the form of a Taylor series. The vertical component of the field on the median plane is expressed as

$$B_y(x,0) = \sum_{n=0}^{\infty} \frac{1}{n!} \left[\frac{d^n B_y}{dx^n}\right]_0 x^n, \tag{1.5.23}$$

where the subscript 0 implies that the derivatives are evaluated at the equilibrium orbit (which is generally at the center of the magnet). n=0 gives the vertical component of the field at the center of the magnet, which is represented as B_0 and the above equation becomes

$$B_y(x,0) = B_0 + \sum_{n=1}^{\infty} \frac{1}{n!} \left[\frac{d^n B_y}{dx^n}\right]_0 x^n, \tag{1.5.24}$$

Similarly, the horizontal component of the field (B_x) on the horizontal axis (X-axis) is expressed as :

$$B_x\,(x,0) = \sum_{n=0}^{\infty} \frac{1}{n!} \left[\frac{d^n B_x}{dx^n}\right]_0 \; x^n. \tag{1.5.25}$$

where, the subscript 0 implies that the derivatives are evaluated at the equilibrium orbit. n=0 gives the horizontal component of the field at the center of the magnet, which is ideally zero in the magnets considered here.

The following are defined :

$$k_n = \frac{1}{B_0\rho}\left[\frac{d^n B_y}{dx^n}\right]_0, \tag{1.5.26a}$$

$$h_n = \frac{1}{B_0\rho}\left[\frac{d^n B_x}{dx^n}\right]_0, \tag{1.5.26b}$$

with ρ as the bending radius of the particle in the magnet and $(B_0\rho)$ as the magnetic rigidity. Therefore, the Eq. (1.5.24) and Eq. (1.5.25) become

$$B_y\,(x,0) = B_0\rho\left(\frac{1}{\rho} + \sum_{n=1}^{\infty} \frac{1}{n!} k_n \; x^n\right), \tag{1.5.27a}$$

$$B_x\,(x,0) = B_0\rho\left(\sum_{n=0}^{\infty} \frac{1}{n!} h_n \; x^n\right). \tag{1.5.27b}$$

k_n and h_n used in the above equations can be related to a_n and b_n given in Eq. (1.5.19) when the horizontal and vertical components of the field are evaluated on the horizontal axis, respectively. Therefore, with $b_0 = 10^4$ and $B_{R_0} = B_0$, one obtains

$$h_n = \frac{10^{-4}\; n!}{\rho\; R_0^n}\; a_n, \tag{1.5.28a}$$

$$k_n = \frac{10^{-4}\; n!}{\rho\; R_0^n}\; b_n. \tag{1.5.28b}$$

The expressions for the horizontal and vertical component of the field in Eq. (1.5.17) can be separated out as

$$B_x = 10^{-4} B_{R_0} \sum_{n=0}^{\infty} \left[b_n \; sin\,(n\theta) \;\; + \;\; a_n \; cos\,(n\theta)\right] \left(\frac{r}{R_0}\right)^n, \tag{1.5.29a}$$

$$B_y = 10^{-4} B_{R_0} \sum_{n=0}^{\infty} \left[b_n \; cos\,(n\theta) \;\; - \;\; a_n \; sin\,(n\theta)\right] \left(\frac{r}{R_0}\right)^n. \tag{1.5.29b}$$

The radial and azimuthal components of the field can be computed by using the following relations :

$$\begin{pmatrix} B_r \\ B_\theta \end{pmatrix} = \begin{pmatrix} cos(\theta) & sin(\theta) \\ -sin(\theta) & cos(\theta) \end{pmatrix} \begin{pmatrix} B_x \\ B_y \end{pmatrix} \tag{1.5.30}$$

Therefore, the radial and azimuthal components of the field can be written as :

$$B_r = 10^{-4} B_{R_0} \sum_{n=0}^{\infty} [b_n \ sin[(n+1)\theta] \ + \ a_n \ cos[(n+1)\theta]] \left(\frac{r}{R_0}\right)^n, \tag{1.5.31a}$$

$$B_\theta = 10^{-4} B_{R_0} \sum_{n=0}^{\infty} [b_n \ cos[(n+1)\theta] \ - \ a_n \ sin[(n+1)\theta]] \left(\frac{r}{R_0}\right)^n. \tag{1.5.31b}$$

In order to represent the vector potential in terms of harmonics, the following relations can be used :

$$B_r = \frac{1}{r}\frac{\partial A_z}{\partial \theta} \quad \text{and} \quad B_\theta = -\frac{\partial A_z}{\partial r},$$

since in the 2-dimensional case $A_x = A_y = 0$. Therefore, on integrating Eqs. (1.5.31) one obtains

$$A_z = -10^{-4} B_{R_0} \sum_{n=0}^{\infty} \left(\frac{R_0}{n+1}\right) [b_n cos[(n+1)\theta] - a_n sin[(n+1)\theta]] \left(\frac{r}{R_0}\right)^{n+1}. \tag{1.5.32}$$

The inverse transform can be used to obtain individual field harmonics at a reference radius R_0 in terms of field or vector potential. For this, first a component of the field or vector potential is evaluated at a radius r and then the integration is performed over the azimuth as follows :

$$a_n = -\frac{10^4}{\pi B_{R_0}} \left(\frac{R_0}{r}\right)^n \int_0^{2\pi} B_y(r,\theta) sin(n\theta) \ d\theta, \tag{1.5.33a}$$

$$= \frac{10^4}{\pi B_{R_0}} \left(\frac{R_0}{r}\right)^n \int_0^{2\pi} B_x(r,\theta) cos(n\theta) \ d\theta, \tag{1.5.33b}$$

$$= \frac{10^4}{\pi B_{R_0}} \left(\frac{R_0}{r}\right)^n \int_0^{2\pi} B_r(r,\theta) cos((n+1)\theta) \ d\theta, \tag{1.5.33c}$$

$$= -\frac{10^4}{\pi B_{R_0}} \left(\frac{R_0}{r}\right)^n \int_0^{2\pi} B_\theta(r,\theta) sin((n+1)\theta) \ d\theta, \tag{1.5.33d}$$

$$= \frac{10^4 (n+1)}{\pi R_0 B_{R_0}} \left(\frac{R_0}{r}\right)^{n+1} \int_0^{2\pi} A_z(r,\theta) sin((n+1)\theta) \ d\theta, \tag{1.5.33e}$$

$$b_n = \frac{10^4}{\pi B_{R_0}} \left(\frac{R_0}{r}\right)^n \int_0^{2\pi} B_y(r,\theta) cos(n\theta) \ d\theta, \tag{1.5.33f}$$

$$= \frac{10^4}{\pi B_{R_0}} \left(\frac{R_0}{r}\right)^n \int_0^{2\pi} B_x(r,\theta) sin(n\theta) \ d\theta, \tag{1.5.33g}$$

$$= \frac{10^4}{\pi B_{R_0}} \left(\frac{R_0}{r}\right)^n \int_0^{2\pi} B_r(r,\theta) sin((n+1)\theta) \ d\theta, \tag{1.5.33h}$$

$$= \frac{10^4}{\pi B_{R_0}} \left(\frac{R_0}{r}\right)^n \int_0^{2\pi} B_\theta(r,\theta) cos((n+1)\theta) \ d\theta, \tag{1.5.33i}$$

$$= -\frac{10^4 (n+1)}{\pi R_0 B_{R_0}} \left(\frac{R_0}{r}\right)^{n+1} \int_0^{2\pi} A_z(r,\theta) cos((n+1)\theta) \ d\theta. \tag{1.5.33j}$$

For the primary harmonic component $n = m$, when the field is perpendicular to the horizontal plane, one obtains

$$b_m = 10^4 \quad \text{and} \quad a_m = 0.$$

1.5.3. Analytic Expressions for Accelerator Magnets

Analytic expressions for the basic cosine theta superconducting magnet design have been previously obtained and described by several authors [12-18,144,175,179]. Superconducting accelerator magnets are usually long cylindrical magnets with the current flowing parallel to the magnet axis (z-axis). The geometry of these magnets is such that one can compute the field in the body of the magnet by assuming that the current is carried by a large number of wires parallel to the z-axis. The total field is obtained by simply superimposing the field created by these wires. For this purpose, it is suitable to carry out a 2-dimensional analysis in the cylindrical coordinate system. A three dimensional analysis will be necessary for computing the field at the ends of the magnet.

Accelerator magnets are designed to produce a well defined field in the aperture of the magnets. The *field* in the aperture is constant for *dipoles*, the *first derivative* of the field is constant for *quadrupoles* and, in general, the n^{th} *derivative* is constant for the n^{th}-order *multipole*. In the following sections, the current distributions needed to produce such multipole fields will be obtained.

1.5.3.1. Field and Vector Potential due to a Line Current

To compute the magnetic field and vector potential due to a single infinitely long wire, it is assumed to carry a current I in the z-direction which is perpendicular to the plane of paper. The field outside this wire at a perpendicular distance R from it will be computed. The cylindrical coordinate system is used to take advantage of the symmetry of the problem.

The magnetic field produced by this wire can be directly calculated by using the integral equation $\oint \vec{H} \cdot d\boldsymbol{s} = I$ (Eqs. (1.5.9)) which gives:

$$H = \frac{I}{2\pi R}, \tag{1.5.34}$$

and in a medium having a relative permeability of μ

$$B = \frac{I\mu\mu_0}{2\pi R}. \tag{1.5.35}$$

The components of vector potential in cylindrical and Cartesian geometry can be written as

$$A_z = \frac{\mu\mu_0 I}{2\pi} ln\left(\frac{1}{R}\right), \tag{1.5.36a}$$

$$A_r = A_\theta = 0, \tag{1.5.36b}$$

$$A_x = A_y = 0. \tag{1.5.36c}$$

The validity of the above relation is verified when the curl of the vector potential is taken to obtain the magnetic field as per Eqs. (1.5.7). This gives $B_r = B_z = 0$ and $B_\theta = \frac{\mu\mu_0 I}{2\pi R}$; which is the same as in Eqs. (1.5.34) with only one component of the field present.

In accelerator magnets, the magnetic field and vector potential are usually expressed in terms of harmonic components. To develop this formalism a line current is assumed to be located at a point "Q" (at $\vec{a}$) and the magnetic field produced by it is computed at point "P" (at $\vec{r}$), as shown in Fig. 1.5.1. The distance between the two is $\vec{R} = \vec{r}$ - $\vec{a}$ with the magnitude $|R| = \sqrt{r^2 + a^2 - 2racos(\theta - \phi)}$.

In this section, the computations will be mostly done in a space free of magnetic material where the relative permeability μ is one. Moreover, to simplify the expressions to follow, Eq. (1.5.36a) is re-written after adding a constant :

$$A_z(r,\theta) = -\frac{\mu_o I}{2\pi} ln\left(\frac{R}{a}\right); \tag{1.5.37}$$

the addition of such a constant does not change the magnetic field which is a derivative of A_z.

Now $A_z(r,\theta)$ will be given in terms of a series expansion containing, in general, summation of terms like $\left(\frac{r}{a}\right)^m$ and $\left(\frac{a}{r}\right)^m$, together with trigonometric functions like $cos(m\theta)$ and $sin(m\theta)$. The exact solution will depend on a particular problem. For example, in the solution of the case when r approaches the origin ($r \to 0$), the $\left(\frac{a}{r}\right)^m$ terms can't be present. Similarly in the solution of the case when r approaches infinity ($r \to \infty$), the $\left(\frac{a}{r}\right)^m$ terms can't be present.

In order to obtain an expansion of the ln in Eq. (1.5.37), the following manipulation is carried out :

$$\begin{aligned} R^2 &= r^2 + a^2 - 2ra\ cos(\theta - \phi), \\ \frac{R}{a} &= \left(1 - \left(\frac{r}{a}\right)e^{i(\phi-\theta)}\right)^{\frac{1}{2}} \cdot \left(1 - \left(\frac{r}{a}\right)e^{-i(\phi-\theta)}\right)^{\frac{1}{2}}, \\ ln\left(\frac{R}{a}\right) &= \frac{1}{2} ln\left(1 - \left(\frac{r}{a}\right)e^{i(\phi-\theta)}\right) + \frac{1}{2} ln\left(1 - \left(\frac{r}{a}\right)e^{-i(\phi-\theta)}\right). \end{aligned}$$

For $|z| < 1$, the logarithmic expansion is given by

$$ln(1-z) = -\left[z + \left(\frac{z^2}{2}\right) + \left(\frac{z^3}{3}\right) + ...\right] = -\sum_{n=1}^{\infty} \frac{z^n}{n}.$$

Therefore, for r < a

$$ln\left(\frac{R}{a}\right) = -\left[\frac{1}{2}\sum_{n=1}^{\infty}\left(\frac{1}{n}\right)\left(\frac{r}{a}\right)^n e^{i\ n(\phi-\theta)} + \frac{1}{2}\sum_{n=1}^{\infty}\left(\frac{1}{n}\right)\left(\frac{r}{a}\right)^n e^{-i\ n(\phi-\theta)}\right],$$

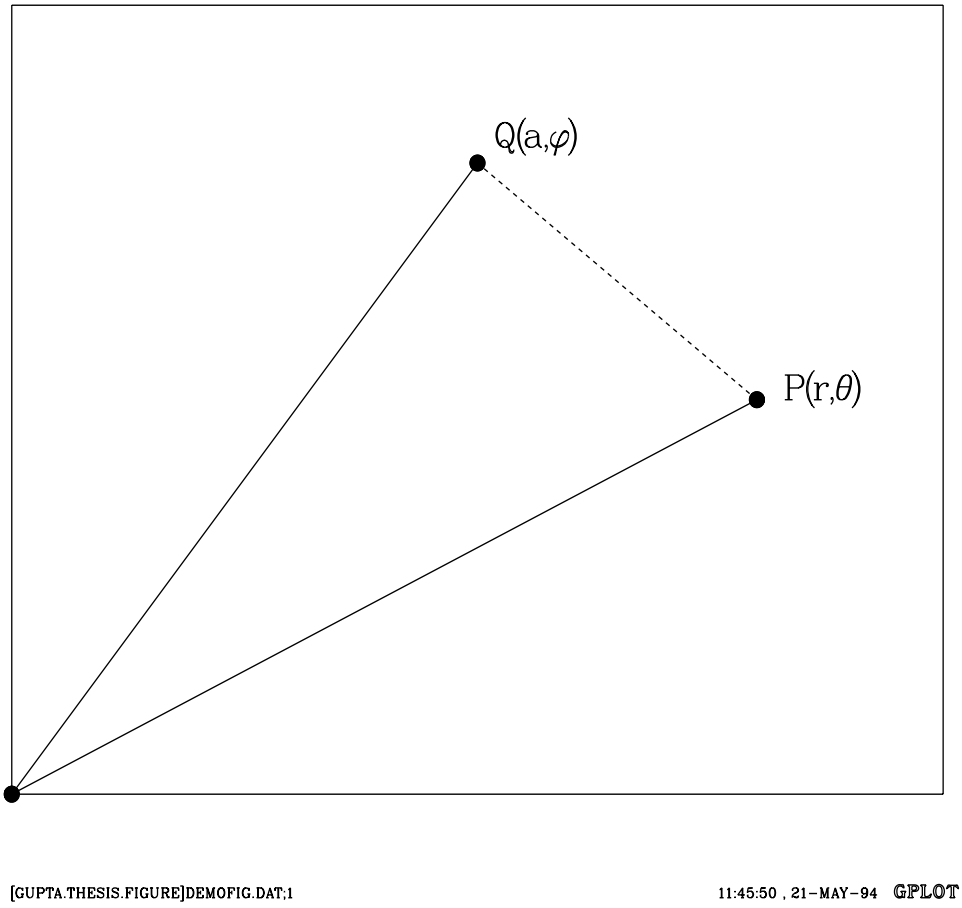

Figure 1.5.1: Computation of the field at a location "P" produced by the line current located at a position "Q".

$$ln\left(\frac{R}{a}\right) = -\sum_{n=1}^{\infty}\left(\frac{1}{n}\right)\left(\frac{r}{a}\right)^{n} cos\left(n\left(\phi-\theta\right)\right). \tag{1.5.38}$$

Substituting Eqs. (1.5.38) in Eqs. (1.5.37) the desired expansion for the vector potential is obtained (for r < a) :

$$A_z\left(r,\theta\right) = \frac{\mu_o I}{2\pi}\sum_{n=1}^{\infty}\left(\frac{1}{n}\right)\left(\frac{r}{a}\right)^{n} cos\left(n\left(\phi-\theta\right)\right). \tag{1.5.39}$$

The magnetic field components are obtained by using Eqs. (1.5.7) and Eqs. (1.5.37) with $A_r = A_\theta = 0$:

$$B_r = \frac{1}{r}\left(\frac{\partial A_z}{\partial \theta}\right), \tag{1.5.40a}$$

$$B_\theta = -\frac{\partial A_z}{\partial r}, \tag{1.5.40b}$$

$$B_z = 0. \tag{1.5.40c}$$

Therefore, for r < a, one would obtain :

$$B_r = \frac{\mu_o I}{2\pi a}\sum_{n=1}^{\infty}\left(\frac{r}{a}\right)^{n-1} sin\left[(n)\left(\phi-\theta\right)\right], \tag{1.5.41a}$$

$$B_\theta = -\frac{\mu_o I}{2\pi a}\sum_{n=1}^{\infty}\left(\frac{r}{a}\right)^{n-1} cos\left[(n)\left(\phi-\theta\right)\right], \tag{1.5.41b}$$

$$B_z = 0. \tag{1.5.41c}$$

In order to compute the harmonics components, the above equations are compared with Eqs. (1.5.31). It should be noted that there the summation starts from $n = 0$ instead of $n = 1$ in Eq. (1.5.39). The following expressions for the normal and skew harmonics at a reference radius R_0 are obtained for a line current located at (a, ϕ) :

$$b_n = 10^4\left(\frac{R_0}{a}\right)^n \; cos\left[(n+1)\,\phi\right], \tag{1.5.42a}$$

$$a_n = -10^4\left(\frac{R_0}{a}\right)^n \; sin\left[(n+1)\,\phi\right], \tag{1.5.42b}$$

and $B_{R_o} = -\frac{\mu_o I}{2\pi a}$.

For r > a case, the following rearrangement is performed to obtain an appropriate expansion :

$$\begin{aligned}
\frac{R}{a} &= \left(\frac{r}{a}\right)\left(1-\left(\frac{a}{r}\right)e^{i(\phi-\theta)}\right)^{\frac{1}{2}}\cdot\left(1-\left(\frac{a}{r}\right)e^{-i(\phi-\theta)}\right)^{\frac{1}{2}},\\
ln\left(\frac{R}{a}\right) &= ln\left(\frac{r}{a}\right)+\left[\frac{1}{2}ln\left(1-\left(\frac{a}{r}\right)e^{i(\phi-\theta)}\right)+\frac{1}{2}ln\left(1-\left(\frac{a}{r}\right)e^{-i(\phi-\theta)}\right)\right],\\
ln\left(\frac{R}{a}\right) &= ln\left(\frac{r}{a}\right)-\left[\frac{1}{2}\sum_{n=1}^{\infty}\left(\frac{1}{n}\right)\left(\frac{a}{r}\right)^n e^{i\;n(\phi-\theta)}+\frac{1}{2}\sum_{n=1}^{\infty}\left(\frac{1}{n}\right)\left(\frac{a}{r}\right)^n e^{-i\;n(\phi-\theta)}\right],\\
ln\left(\frac{R}{a}\right) &= ln\left(\frac{r}{a}\right)-\sum_{n=1}^{\infty}\left(\frac{1}{n}\right)\left(\frac{a}{r}\right)^n cos\left(n\left(\phi-\theta\right)\right).
\end{aligned} \tag{1.5.43}$$

Therefore, for r > a, one obtains the following expression for the vector potential :

$$A_z\left(r,\theta\right) = -\frac{\mu_o I}{2\pi}ln\left(\frac{r}{a}\right)+\frac{\mu_o I}{2\pi}\sum_{n=1}^{\infty}\left(\frac{1}{n}\right)\left(\frac{a}{r}\right)^n cos\left(n\left(\phi-\theta\right)\right). \tag{1.5.44}$$

The magnetic field components are obtained by using Eqs. (1.5.40) :

$$B_r = \frac{\mu_o I}{2\pi a} \sum_{n=0}^{\infty} \left(\frac{a}{r}\right)^{n+1} sin\left(n\left(\phi - \theta\right)\right), \tag{1.5.45a}$$

$$B_\theta = \frac{\mu_o I}{2\pi a} \sum_{n=0}^{\infty} \left(\frac{a}{r}\right)^{n+1} cos\left(n\left(\phi - \theta\right)\right), \tag{1.5.45b}$$

$$B_z = 0. \tag{1.5.45c}$$

It may be noted that in the expression for B_θ, the summation in n starts from $n = 0$ instead of $n = 1$. The (B_x, B_y) components of the field can be computed using the following relation:

$$\begin{pmatrix} B_x \\ B_y \end{pmatrix} = \begin{pmatrix} cos\left(\theta\right) & -sin\left(\theta\right) \\ sin\left(\theta\right) & cos\left(\theta\right) \end{pmatrix} \begin{pmatrix} B_r \\ B_\theta \end{pmatrix}. \tag{1.5.46}$$

1.5.3.2. Line Current in a Cylindrical Iron Cavity

Expressions are obtained here for the vector potential and magnetic field due to an infinitely long paraxial filament of current I at a radius a in a cylindrical cavity having a radius $R_f > a$. The iron is infinitely long and infinitely thick and has a constant relative permeability μ, which is referred to here simply as permeability following the convention explained earlier. The method of image currents can be applied to include the contribution from the iron [179]. The expressions are obtained here by matching the boundary conditions at the interface of the air and iron boundary [19]. General expressions for the vector potential and the components of the field in the region $a < r < R_f$, are given by :

$$A_z(r,\theta) = -\frac{\mu_o I}{2\pi} ln\left(\frac{r}{a}\right) + \frac{\mu_o I}{2\pi}\sum_{n=1}^{\infty}\left(\frac{1}{n}\right)\left(\frac{a}{r}\right)^n cos\left(n\left(\phi-\theta\right)\right) + \mu_o\sum_{n=1}^{\infty} E_n r^n cos\left(n\left(\phi-\theta\right)\right), \tag{1.5.47}$$

$$B_r = \frac{\mu_o I}{2\pi a}\sum_{n=1}^{\infty}\left(\frac{a}{r}\right)^{n+1} sin\left(n\left(\phi-\theta\right)\right) + \mu_o\sum_{n=1}^{\infty} nE_n r^{n-1} sin\left(n\left(\phi-\theta\right)\right), \tag{1.5.48a}$$

$$H_\theta = \frac{I}{2\pi a}\sum_{n=0}^{\infty}\left(\frac{a}{r}\right)^{n+1} cos\left(n\left(\phi-\theta\right)\right) - \sum_{n=1}^{\infty} nE_n r^{n-1} cos\left(n\left(\phi-\theta\right)\right), \tag{1.5.48b}$$

and in the region $r > R_f$:

$$A_z(r,\theta) = \mu\mu_o F_o ln\left(\frac{r}{a}\right) + \mu\mu_o\sum_{n=1}^{\infty} F_n\left(\frac{1}{r}\right)^n cos\left(n\left(\phi-\theta\right)\right), \tag{1.5.49}$$

$$B_r = \mu\mu_o\sum_{n=1}^{\infty} nF_n\left(\frac{1}{r}\right)^{n+1} sin\left(n\left(\phi-\theta\right)\right), \tag{1.5.50a}$$

$$H_\theta = -\frac{F_o}{r} + \sum_{n=1}^{\infty} nF_n\left(\frac{1}{r}\right)^{n+1} cos\left(n\left(\phi-\theta\right)\right), \tag{1.5.50b}$$

where E_n and F_n are coefficients which can be determined by the boundary conditions at $r = R_f$ that

$$\left(B_r\right)_{air} = \left(B_r\right)_{iron},$$

$$\left(H_\theta\right)_{air} = \left(H_\theta\right)_{iron},$$

i.e. the normal component of B and the azimuthal component of H are continuous. Therefore, the required boundary conditions at $r = R_f$ for $n \neq 0$ gives :

$$\frac{\mu_o I}{2\pi a}\left(\frac{a}{R_f}\right)^{n+1} + n\ \mu_o\ E_n {R_f}^{n-1} = n\ \mu_0\ \mu\ F_n\left(\frac{1}{R_f}\right)^{n+1},$$
$$\frac{I}{2\pi a}\left(\frac{a}{R_f}\right)^{n+1} - \ n\ E_n {R_f}^{n-1} = n\ F_n\left(\frac{1}{R_f}\right)^{n+1},$$

which gives

$$E_n = \frac{1}{n}\frac{\mu - 1}{\mu + 1}\ \frac{I}{2\pi}\ \left(\frac{a}{R_f^2}\right)^n, \tag{1.5.51a}$$

$$F_n = \frac{1}{n}\frac{2}{\mu + 1}\ \frac{I}{2\pi a}\ a^{n+1}. \tag{1.5.51b}$$

The $n = 0$ term appears only in the expression for H_θ and on matching the boundary condition, one obtains :

$$\frac{I}{2\pi R_f} = -\frac{F_o}{R_f},$$

which gives

$$F_o = -\frac{I}{2\pi}. \tag{1.5.52}$$

The expressions for vector potential and field components for $a < r < R_f$ case are obtained when E_n from Eq. (1.5.51a) is substituted in Eq. (1.5.47) and Eqs. (1.5.48) :

$$A_z(r,\theta) = -\frac{\mu_o I}{2\pi} ln\left(\frac{r}{a}\right) + \frac{\mu_o I}{2\pi}\sum_{n=1}^{\infty}\frac{1}{n}\left(\frac{a}{r}\right)^n cos\left(n\left(\phi - \theta\right)\right)\left[1 + \frac{\mu - 1}{\mu + 1}\left(\frac{r}{R_f}\right)^{2n}\right], \tag{1.5.53}$$

$$B_r = \frac{\mu_o I}{2\pi a}\sum_{n=1}^{\infty}\left(\frac{a}{r}\right)^{n+1} sin\left(n\left(\phi - \theta\right)\right)\left[1 + \frac{\mu - 1}{\mu + 1}\left(\frac{r}{R_f}\right)^{2n}\right], \tag{1.5.54a}$$

$$B_\theta = \frac{\mu_o I}{2\pi r} + \frac{\mu_o I}{2\pi a}\sum_{n=1}^{\infty}\left(\frac{a}{r}\right)^{n+1} cos\left(n\left(\phi - \theta\right)\right)\left[1 - \frac{\mu - 1}{\mu + 1}\left(\frac{r}{R_f}\right)^{2n}\right]. \tag{1.5.54b}$$

In the above equations, the second term in the square brackets is the additional contribution of the iron to the field produced by the coil.

To obtain the expressions for the vector potential and field for $r < a$ it must be noted that a current filament is present at $r = a$. However, the radial component of the field B_r must still be continuous, i.e. at $r = a$

$$B_r\left(in\right) = B_r\left(out\right),$$

where $B_r(in)$ and $B_r(out)$ are the magnetic induction for $r < a$ and $a < r < R_f$ respectively. The presence of the source (current), however, gives a discontinuity in the azimuthal component of the field H_θ with $H_\theta(in)$ - $H_\theta(out)$ determined by the current density at $r = a$. A general expression for the vector potential for $r < a$ is given by (see Eq. (1.5.39)) :

$$A_z(r,\theta) = \mu_o \sum_{n=1}^{\infty} I_n \; r^n cos\left(n\left(\phi - \theta\right)\right), \tag{1.5.55}$$

where the I_n are unknown coefficients. Using Eqs. (1.5.40) :

$$B_r = \mu_o \sum_{n=1}^{\infty} I_n \;\; n \;\; r^{n-1} sin\left(n\left(\phi - \theta\right)\right), \tag{1.5.56a}$$

$$B_\theta = -\mu_o \sum_{n=1}^{\infty} I_n \;\; n \;\; r^{n-1} cos\left(n\left(\phi - \theta\right)\right), \tag{1.5.56b}$$

$$B_z = 0. \tag{1.5.56c}$$

In order for B_r to be continuous at $r = a$ one obtains from Eq. (1.5.56a) and Eq. (1.5.54a) :

$$I_n = \frac{I}{2\pi}\left(\frac{1}{n}\right)\left(\frac{1}{a}\right)^n \left[1 + \frac{\mu - 1}{\mu + 1}\left(\frac{a}{R_f}\right)^{2n}\right]. \tag{1.5.57}$$

Using this in Eqs. (1.5.56) gives the expressions for the field and vector potential for $r < a$ as :

$$A_z(r,\theta) = \frac{\mu_o I}{2\pi} \sum_{n=1}^{\infty} \left(\frac{1}{n}\right)\left(\frac{r}{a}\right)^n cos\left(n\left(\phi - \theta\right)\right)\left[1 + \frac{\mu - 1}{\mu + 1}\left(\frac{a}{R_f}\right)^{2n}\right]. \tag{1.5.58}$$

$$B_r = \frac{\mu_o I}{2\pi a} \sum_{n=1}^{\infty} \left(\frac{r}{a}\right)^{n-1} sin\left(n\left(\phi - \theta\right)\right)\left[1 + \frac{\mu - 1}{\mu + 1}\left(\frac{a}{R_f}\right)^{2n}\right], \tag{1.5.59a}$$

$$B_\theta = -\frac{\mu_o I}{2\pi a} \sum_{n=1}^{\infty} \left(\frac{r}{a}\right)^{n-1} cos\left(n\left(\phi - \theta\right)\right)\left[1 + \frac{\mu - 1}{\mu + 1}\left(\frac{a}{R_f}\right)^{2n}\right], \tag{1.5.59b}$$

$$B_z = 0. \tag{1.5.59c}$$

To compute the field harmonics the procedure of Eqs. (1.5.42) is repeated. As before, the summation over n in the above is now changed so that it starts from n=0 instead of n=1.

$$b_n = 10^4 \left(\frac{R_0}{a}\right)^n \;\; cos\left(\left(n+1\right)\phi\right)\left[1 + \frac{\mu - 1}{\mu + 1}\left(\frac{a}{R_f}\right)^{2(n+1)}\right], \tag{1.5.60a}$$

$$a_n = -10^4 \left(\frac{R_0}{a}\right)^n \;\; sin\left(\left(n+1\right)\phi\right)\left[1 + \frac{\mu - 1}{\mu + 1}\left(\frac{a}{R_f}\right)^{2(n+1)}\right]. \tag{1.5.60b}$$

All expressions derived so far reproduce the results obtained from the method of images [179] which says that the effect of iron can be replaced by an additional line current $I^{'}$ located at $(a^{'}, \phi)$ with

$$I^{'} = \left(\frac{\mu - 1}{\mu + 1}\right) I,$$
$$a^{'} = \frac{R_f^2}{a}.$$

The expressions for vector potential and field components for $r > R_f$ case are obtained when F_n from Eq. (1.5.51b) and Eq. (1.5.52) are substituted in Eqs. (1.5.49) and Eqs. (1.5.50) :

$$A_z(r,\theta) = -\frac{\mu\mu_o I}{2\pi} ln\left(\frac{r}{a}\right) + \frac{2\mu}{\mu+1}\frac{\mu_o I}{2\pi}\sum_{n=1}^{\infty}\left(\frac{1}{n}\right)\left(\frac{a}{r}\right)^n cos\left(n\left(\phi-\theta\right)\right) \qquad (1.5.61)$$

$$B_r = \frac{2\mu}{\mu+1}\frac{\mu_o I}{2\pi a}\sum_{n=1}^{\infty}\left(\frac{a}{r}\right)^{n+1} sin\left(n\left(\phi-\theta\right)\right), \qquad (1.5.62a)$$

$$B_\theta = \frac{\mu\mu_o I}{2\pi r} + \frac{2\mu}{\mu+1}\frac{\mu_o I}{2\pi a}\sum_{n=1}^{\infty}\left(\frac{a}{r}\right)^{n+1} cos\left(n\left(\phi-\theta\right)\right). \qquad (1.5.62b)$$

1.5.3.3. Line Current in a Cylindrical Iron Shell

In deriving the expressions for the vector potential and field due to a line current inside an cylindrical iron it was assumed in the last section that the iron outer boundary extends to infinity. This is, however, not the case in practice. If the outer diameter of the cylindrical iron shell is R_a, then the general expressions for the vector potential in the various regions are given by :

$$A_z(r,\theta) = \mu_o \sum_{n=1}^{\infty} I_n^{'}\ r^n cos\left(n\left(\phi-\theta\right)\right), \qquad [for \quad \mathrm{r} < \mathrm{a}] \tag{1.5.63a}$$

$$A_z(r,\theta) = -\frac{\mu_o I}{2\pi} ln\left(\frac{r}{a}\right) + \frac{\mu_o I}{2\pi} \sum_{n=1}^{\infty} \left(\frac{1}{n}\right)\left(\frac{a}{r}\right)^n cos\left(n\left(\phi-\theta\right)\right) + \mu_o \sum_{n=1}^{\infty} E_n^{'} r^n cos\left(n\left(\phi-\theta\right)\right), \qquad [for \quad \mathrm{a} < \mathrm{r} < \mathrm{R_f}] \tag{1.5.63b}$$

$$A_z(r,\theta) = \mu\mu_o F_o^{'} ln\left(\frac{r}{a}\right) + \mu\mu_o \sum_{n=1}^{\infty} F_n^{'} \left(\frac{1}{r}\right)^n cos\left(n\left(\phi-\theta\right)\right) + \mu\mu_o \sum_{n=1}^{\infty} G_n^{'} r^n cos\left(n\left(\phi-\theta\right)\right), \qquad [for \quad \mathrm{R_f} < \mathrm{r} < \mathrm{R_a}] \tag{1.5.63c}$$

$$A_z(r,\theta) = \mu_o H_o^{'} ln\left(\frac{r}{a}\right) + \mu_o \sum_{n=1}^{\infty} H_n^{'} \left(\frac{1}{r}\right)^n cos\left(n\left(\phi-\theta\right)\right), \qquad [for \quad \mathrm{r} > \mathrm{R_a}] \tag{1.5.63d}$$

Following an approach similar to one used in previous section, the five coefficients ($E_n^{'}$, $F_n^{'}$, $G_n^{'}$, $H_n^{'}$, $I_n^{'}$) are obtained by matching the five boundary conditions (B_r is continuous at $r = a$, $r = R_f$ and $r = R_a$ and B_θ is continuous at $r = R_f$ and $r = R_a$). The results of that exercise for $n > 0$ are given here :

$$I_n^{'} = \frac{I}{2\pi}\left(\frac{1}{n}\right)\left(\frac{1}{a}\right)^n \left[1 + \frac{\mu-1}{\mu+1}\left(\frac{a}{R_f}\right)^{2n} \frac{\left[1-\left(\frac{R_f}{R_a}\right)^{2n}\right]}{\left[1-\left(\frac{\mu-1}{\mu+1}\right)^2\left(\frac{R_f}{R_a}\right)^{2n}\right]}\right] \quad , \tag{1.5.64a}$$

$$E_n^{'} = \frac{1}{n}\frac{\mu-1}{\mu+1}\ \frac{I}{2\pi}\ \left(\frac{a}{R_f^2}\right)^n \frac{\left[1-\left(\frac{R_f}{R_a}\right)^{2n}\right]}{\left[1-\left(\frac{\mu-1}{\mu+1}\right)^2\left(\frac{R_f}{R_a}\right)^{2n}\right]} \quad , \tag{1.5.64b}$$

$$F_n^{'} = \frac{1}{\mu+1}\ \frac{I}{n\pi}\ \frac{a^n}{\left[1-\left(\frac{\mu-1}{\mu+1}\right)^2\left(\frac{R_f}{R_a}\right)^{2n}\right]} \quad , \tag{1.5.64c}$$

$$G_n^{'} = -\frac{(\mu-1)}{(\mu+1)^2}\ \frac{I}{n\pi}\frac{\left(\frac{a}{R_a^2}\right)^n}{\left[1-\left(\frac{\mu-1}{\mu+1}\right)^2\left(\frac{R_f}{R_a}\right)^{2n}\right]}\quad , \tag{1.5.64d}$$

$$H_n^{'} = \frac{2\mu}{(\mu+1)^2}\ \frac{I}{n\pi}\ \frac{a^n}{\left[1-\left(\frac{\mu-1}{\mu+1}\right)^2\left(\frac{R_f}{R_a}\right)^{2n}\right]}\quad , \tag{1.5.64e}$$

and for $n = 0$, the terms are:

$$F_o^{'} \ = \ H_o^{'} = -\frac{I}{2\pi}. \tag{1.5.65}$$

Therefore, the expressions for the vector potential and field components in various regions due to a line current I at (a,θ) inside a cylindrical iron shell having inner radius R_f and outer radius R_a are given as follows (in each case $B_z(r,\theta)=0$) :

Inside Coil($\mathbf{r < a}$)

$$A_z(r,\theta) = \frac{\mu_o I}{2\pi}\sum_{n=1}^{\infty}\left(\frac{1}{n}\right)\left[1+\frac{\mu-1}{\mu+1}\left(\frac{a}{R_f}\right)^{2n}\frac{\left[1-\left(\frac{R_f}{R_a}\right)^{2n}\right]}{\left[1-\left(\frac{\mu-1}{\mu+1}\right)^2\left(\frac{R_f}{R_a}\right)^{2n}\right]}\right]\times$$
$$\left(\frac{r}{a}\right)^n cos\left(n\left(\phi-\theta\right)\right)\quad . \tag{1.5.66}$$

$$B_r = \frac{\mu_o I}{2\pi a}\sum_{n=1}^{\infty}\left[1+\frac{\mu-1}{\mu+1}\left(\frac{a}{R_f}\right)^{2n}\frac{\left[1-\left(\frac{R_f}{R_a}\right)^{2n}\right]}{\left[1-\left(\frac{\mu-1}{\mu+1}\right)^2\left(\frac{R_f}{R_a}\right)^{2n}\right]}\right]\times$$
$$\left(\frac{r}{a}\right)^{n-1} sin\left(n\left(\phi-\theta\right)\right)\quad , \tag{1.5.67a}$$

$$B_\theta = -\frac{\mu_o I}{2\pi a}\sum_{n=1}^{\infty}\left[1+\frac{\mu-1}{\mu+1}\left(\frac{a}{R_f}\right)^{2n}\frac{\left[1-\left(\frac{R_f}{R_a}\right)^{2n}\right]}{\left[1-\left(\frac{\mu-1}{\mu+1}\right)^2\left(\frac{R_f}{R_a}\right)^{2n}\right]}\right]\times$$
$$\left(\frac{r}{a}\right)^{n-1} cos\left(n\left(\phi-\theta\right)\right)\quad , \tag{1.5.67b}$$

Between Coil and Iron ($\mathbf{a < r < R_f}$)

$$A_z(r,\theta) = -\frac{\mu_o I}{2\pi}ln\left(\frac{r}{a}\right)+\frac{\mu_o I}{2\pi}\sum_{n=1}^{\infty}\left(\frac{1}{n}\right)\left(1+\frac{\frac{\mu-1}{\mu+1}\left(\frac{r}{R_f}\right)^{2n}\left[1-\left(\frac{R_f}{R_a}\right)^{2m}\right]}{1-\left(\frac{\mu-1}{\mu+1}\right)^2\left(\frac{R_f}{R_a}\right)^{2n}}\right)\times$$
$$\left(\frac{a}{r}\right)^n cos\left(n\left(\phi-\theta\right)\right)\ , \tag{1.5.68}$$

$$B_r = \frac{\mu_o I}{2\pi a}\sum_{n=1}^{\infty}\left(1+\frac{\frac{\mu-1}{\mu+1}\left(\frac{r}{R_f}\right)^{2n}\left[1-\left(\frac{R_f}{R_a}\right)^{2m}\right]}{1-\left(\frac{\mu-1}{\mu+1}\right)^2\left(\frac{R_f}{R_a}\right)^{2n}}\right)\times$$

$$\left(\frac{a}{r}\right)^{n+1} sin\left(n\left(\phi-\theta\right)\right) \quad , \tag{1.5.69a}$$

$$B_\theta = \frac{\mu_o I}{2\pi r} + \frac{\mu_o I}{2\pi a}\sum_{n=1}^{\infty}\left(1 - \frac{\frac{\mu-1}{\mu+1}\left(\frac{r}{R_f}\right)^{2n}\left[1-\left(\frac{R_f}{R_a}\right)^{2m}\right]}{1-\left(\frac{\mu-1}{\mu+1}\right)^2\left(\frac{R_f}{R_a}\right)^{2n}}\right)\times$$

$$\left(\frac{a}{r}\right)^{n+1} cos\left(n\left(\phi-\theta\right)\right) \quad . \tag{1.5.69b}$$

Inside Iron ($\mathbf{R_f < r < R_a}$)

$$A_z\left(r,\theta\right) = -\frac{\mu\mu_o I}{2\pi} ln\left(\frac{r}{a}\right) + \frac{\mu\mu_o I}{\pi\left(\mu+1\right)}\sum_{n=1}^{\infty}\left(\frac{1}{n}\right)\frac{1-\frac{\mu-1}{\mu+1}\left(\frac{r}{R_a}\right)^{2n}}{1-\left(\frac{\mu-1}{\mu+1}\right)^2\left(\frac{R_f}{R_a}\right)^{2n}}\times$$

$$\left(\frac{a}{r}\right)^{n} cos\left(n\left(\phi-\theta\right)\right) \quad , \tag{1.5.70}$$

$$B_r = \frac{\mu\mu_o I}{\pi a\left(\mu+1\right)}\sum_{n=1}^{\infty}\frac{1-\frac{\mu-1}{\mu+1}\left(\frac{r}{R_a}\right)^{2n}}{1-\left(\frac{\mu-1}{\mu+1}\right)^2\left(\frac{R_f}{R_a}\right)^{2n}}\times$$

$$\left(\frac{a}{r}\right)^{n+1} sin\left(n\left(\phi-\theta\right)\right) \quad , \tag{1.5.71a}$$

$$B_\theta = \frac{\mu\mu_o I}{2\pi r} + \frac{\mu\mu_o I}{\pi a\left(\mu+1\right)}\sum_{n=1}^{\infty}\frac{1+\frac{\mu-1}{\mu+1}\left(\frac{r}{R_a}\right)^{2n}}{1-\left(\frac{\mu-1}{\mu+1}\right)^2\left(\frac{R_f}{R_a}\right)^{2n}}\times$$

$$\left(\frac{a}{r}\right)^{n+1} cos\left(n\left(\phi-\theta\right)\right) \quad . \tag{1.5.71b}$$

Outside Iron ($\mathbf{r > R_a}$)

$$A_z\left(r,\theta\right) = -\frac{\mu_o I}{2\pi} ln\left(\frac{r}{a}\right) + \frac{2\mu\mu_o I}{\pi\left(\mu+1\right)^2}\sum_{n=1}^{\infty}\frac{1}{1-\left(\frac{\mu-1}{\mu+1}\right)^2\left(\frac{R_f}{R_a}\right)^{2n}}\times$$

$$\left(\frac{1}{n}\right)\left(\frac{a}{r}\right)^{n} cos\left(n\left(\phi-\theta\right)\right) \tag{1.5.72}$$

$$B_r = \frac{2\mu}{\left(\mu+1\right)^2}\frac{\mu_o I}{\pi a}\sum_{n=1}^{\infty}\frac{1}{1-\left(\frac{\mu-1}{\mu+1}\right)^2\left(\frac{R_f}{R_a}\right)^{2n}}\times$$

$$\left(\frac{a}{r}\right)^{n+1} sin\left(n\left(\phi-\theta\right)\right), \tag{1.5.73a}$$

$$B_\theta = \frac{\mu_o I}{2\pi r} + \frac{2\mu}{\left(\mu+1\right)^2}\frac{\mu_o I}{\pi a}\sum_{n=0}^{\infty}\frac{1}{1-\left(\frac{\mu-1}{\mu+1}\right)^2\left(\frac{R_f}{R_a}\right)^{2n}}\times$$

$$\left(\frac{a}{r}\right)^{n+1} cos\left(n\left(\phi-\theta\right)\right). \tag{1.5.73b}$$

Field Harmonics

The field harmonics are given by :

$$b_n = 10^4 \left(\frac{R_0}{a}\right)^n \; cos\left((n+1)\,\phi\right) \left[1 + \frac{\mu-1}{\mu+1}\left(\frac{a}{R_f}\right)^{2(n+1)} \frac{1-\left(\frac{R_f}{R_a}\right)^{2(n+1)}}{1-\left(\frac{\mu-1}{\mu+1}\right)^2\left(\frac{R_f}{R_a}\right)^{2(n+1)}}\right], \qquad (1.5.74a)$$

$$a_n = -10^4 \left(\frac{R_0}{a}\right)^n \; sin\left((n+1)\,\phi\right) \left[1 + \frac{\mu-1}{\mu+1}\left(\frac{a}{R_f}\right)^{2(n+1)} \frac{1-\left(\frac{R_f}{R_a}\right)^{2(n+1)}}{1-\left(\frac{\mu-1}{\mu+1}\right)^2\left(\frac{R_f}{R_a}\right)^{2(n+1)}}\right]. \qquad (1.5.74b)$$

1.5.3.4. Field and Harmonics due to Current Blocks in Air

The expressions derived for the line current in the section 1.5.3.1 are extended here for one or more blocks of current. The geometry of the problem is such that a wire is replaced by a radial block between radii ρ_1 and ρ_2 and angle ϕ_1 and ϕ_2. The block has a constant current density J such that the total current is still I with $I = \frac{1}{2}J(\rho_2^2 - \rho_1^2)(\phi_2 - \phi_1)$. To compute the vector potential and component of field at (r, θ) Eq. (1.5.36) and Eqs. (1.5.41) should be integrated [179] as (for $r < \rho_1$) :

$$A_z(r,\theta) = \sum_{n=1}^{\infty} \int_{\rho_1}^{\rho_2} \frac{\mu_o J}{2\pi} \left(\frac{1}{n}\right) \left(\frac{r}{a}\right)^n a \; da \int_{\phi_1}^{\phi_2} cos\left[n\left(\phi - \theta\right)\right] \; d\phi, \tag{1.5.75}$$

$$B_r(r,\theta) = \sum_{n=1}^{\infty} \int_{\rho_1}^{\rho_2} \frac{\mu_o J}{2\pi a} \left(\frac{r}{a}\right)^{n-1} a \; da \int_{\phi_1}^{\phi_2} sin\left[n\left(\phi - \theta\right)\right] d\phi, \tag{1.5.76a}$$

$$B_\theta(r,\theta) = -\sum_{n=1}^{\infty} \int_{\rho_1}^{\rho_2} \frac{\mu_o J}{2\pi a} \left(\frac{r}{a}\right)^{n-1} a \; da \int_{\phi_1}^{\phi_2} cos\left[n\left(\phi - \theta\right)\right] \; d\phi. \tag{1.5.76b}$$

The integration of the above equations for the vector potential and the field components gives :

$$\begin{aligned} A_z(r,\theta) = {} & \frac{\mu_o J r}{2\pi}(\rho_2 - \rho_1)\left[sin\left(\phi_2 - \theta\right) - sin\left(\phi_1 - \theta\right)\right] \\ & + \frac{\mu_o J r^2}{8\pi} ln\left(\frac{\rho_2}{\rho_1}\right)\left[sin\left(2\left(\phi_2 - \theta\right)\right) - sin\left(2\left(\phi_1 - \theta\right)\right)\right] \\ & - \frac{\mu_o J}{2\pi} \sum_{n=3}^{\infty} \frac{r^n}{n^2\left(n-2\right)} \left(\frac{1}{\rho_2^{n-2}} - \frac{1}{\rho_1^{n-2}}\right) \quad \times \\ & \qquad \left[sin\left(n\left(\phi_2 - \theta\right)\right) - sin\left(n\left(\phi_1 - \theta\right)\right)\right], \end{aligned} \tag{1.5.77}$$

$$\begin{aligned} B_r(r,\theta) = {} & -\frac{\mu_o J}{2\pi}(\rho_2 - \rho_1)\left[cos\left(\phi_2 - \theta\right) - cos\left(\phi_1 - \theta\right)\right] \\ & - \frac{\mu_o J r}{4\pi} ln\left(\frac{\rho_2}{\rho_1}\right)\left[cos\left(2\left(\phi_2 - \theta\right)\right) - cos\left(2\left(\phi_1 - \theta\right)\right)\right] \\ & + \frac{\mu_o J}{2\pi} \sum_{n=3}^{\infty} \frac{r^{n-1}}{n\left(n-2\right)} \left(\frac{1}{\rho_2^{n-2}} - \frac{1}{\rho_1^{n-2}}\right) \quad \times \\ & \qquad \left[cos\left(n\left(\phi_2 - \theta\right)\right) - cos\left(n\left(\phi_1 - \theta\right)\right)\right], \end{aligned} \tag{1.5.78a}$$

$$\begin{aligned} B_\theta(r,\theta) = {} & -\frac{\mu_o J}{2\pi}(\rho_2 - \rho_1)\left[sin\left(\phi_2 - \theta\right) - sin\left(\phi_1 - \theta\right)\right] \\ & - \frac{\mu_o J r}{4\pi} ln\left(\frac{\rho_2}{\rho_1}\right)\left[sin\left(2\left(\phi_2 - \theta\right)\right) - sin\left(2\left(\phi_1 - \theta\right)\right)\right] \\ & + \frac{\mu_o J}{2\pi} \sum_{n=3}^{\infty} \frac{r^{n-1}}{n\left(n-2\right)} \left(\frac{1}{\rho_2^{n-2}} - \frac{1}{\rho_1^{n-2}}\right) \quad \times \\ & \qquad \left[sin\left(n\left(\phi_2 - \theta\right)\right) - sin\left(n\left(\phi_1 - \theta\right)\right)\right]. \end{aligned} \tag{1.5.78b}$$

Now the harmonics components a_n and b_n (the dimensionless coefficients as defined in Eqs. (1.5.31)) are computed due to the field from a single current block. It should be

noted that the summation of a_n and b_n starts from $n = 0$ instead of $n = 1$ in Eq. (1.5.78). For $n > 1$ and harmonics normalized to the dipole field, the following expressions for the normal and skew harmonics at a reference radius R_o are obtained using the procedure of Eqs. (1.5.42) :

$$b_n = \frac{-10^4 R_0^n}{(n^2-1)} \left[\left(\frac{1}{\rho_2^{n-1}} - \frac{1}{\rho_1^{n-1}} \right) / (\rho_2 - \rho_1) \right] \frac{sin\left((n+1)\phi_2\right) - sin\left((n+1)\phi_1\right)}{sin\left(\phi_2\right) - sin\left(\phi_1\right)}, \tag{1.5.79a}$$

$$a_n = \frac{-10^4 R_0^n}{(n^2-1)} \left[\left(\frac{1}{\rho_2^{n-1}} - \frac{1}{\rho_1^{n-1}} \right) / (\rho_2 - \rho_1) \right] \frac{cos\left((n+1)\phi_2\right) - cos\left((n+1)\phi_1\right)}{sin\left(\phi_2\right) - sin\left(\phi_1\right)}, \tag{1.5.79b}$$

and the harmonic expressions for $n = 1$ are

$$b_n = \frac{10^4 R_0 ln\left(\frac{\rho_2}{\rho_1}\right)}{\rho_2 - \rho_1} \frac{sin\left(2\phi_2\right) - sin\left(2\phi_1\right)}{sin\left(\phi_2\right) - sin\left(\phi_1\right)}, \tag{1.5.80a}$$

$$a_n = \frac{10^4 R_0 ln\left(\frac{\rho_2}{\rho_1}\right)}{\rho_2 - \rho_1} \frac{cos\left(2\phi_2\right) - cos\left(2\phi_1\right)}{sin\left(\phi_2\right) - sin\left(\phi_1\right)}. \tag{1.5.80b}$$

To compute A_n and B_n (having the dimensions of field and defined in Eqs. (1.5.21)) one derives the expressions for field components from Eqs. (1.5.78) at a reference radius R_o in the form of :

$$B_r = \sum_{n=1}^{\infty} \left(\frac{r}{R_o} \right)^{n-1} \left[B_n \ sin\left(n\theta\right) \ + \ A_n \ cos\left(n\theta\right) \right], \tag{1.5.81a}$$

$$B_\theta = \sum_{n=1}^{\infty} \left(\frac{r}{R_o} \right)^{n-1} \left[B_n \ cos\left(n\theta\right) \ - \ A_n \ sin\left(n\theta\right) \right], \tag{1.5.81b}$$

to obtain

$$A_1 = -\frac{\mu_o J}{2\pi} (\rho_2 - \rho_1) \left[cos\left(\phi_2\right) - cos\left(\phi_1\right) \right], \tag{1.5.82a}$$

$$A_2 = -\frac{\mu_o J R_o}{2\pi} ln\left(\frac{\rho_2}{\rho_1}\right) \left[cos\left(2\phi_2\right) - cos\left(2\phi_1\right) \right], \tag{1.5.82b}$$

for n $\geq$ 3

$$A_n = \frac{\mu_o J}{2\pi} \frac{R_o^{n-1}}{n\left(n-2\right)} \left(\frac{1}{\rho_2^{n-2}} - \frac{1}{\rho_1^{n-2}} \right) \left[cos\left(n\phi_2\right) - cos\left(n\phi_1\right) \right], \tag{1.5.82c}$$

and

$$B_1 = -\frac{\mu_o J}{2\pi} (\rho_2 - \rho_1) \left[sin\left(\phi_2\right) - sin\left(\phi_1\right) \right], \tag{1.5.83a}$$

$$B_2 = -\frac{\mu_o J R_o}{2\pi} ln\left(\frac{\rho_2}{\rho_1}\right) \left[sin\left(2\phi_2\right) - sin\left(2\phi_1\right) \right], \tag{1.5.83b}$$

for n $\geq$ 3

$$B_n = \frac{\mu_o J}{2\pi} \sum_{n=3}^{\infty} \frac{R_o^{n-1}}{n\left(n-2\right)} \left(\frac{1}{\rho_2^{n-2}} - \frac{1}{\rho_1^{n-2}} \right) \left[sin\left(n\phi_2\right) - sin\left(n\phi_1\right) \right]. \tag{1.5.83c}$$

In a typical superconducting magnet several current blocks are used to generate the desired multipolar field. In order to compute the harmonics due to several current blocks, the field and field harmonics A_n and B_n (coefficients having the dimension of field) can be directly superimposed. However, a_n and b_n (dimensionless coefficients) can not be directly added and they must be obtained from A_n and B_n as follows :

$$b_n = 10^4 \frac{\sum_k (B_{n+1})_k}{\sum_k (B_{m+1})_k}, \tag{1.5.84a}$$

$$a_n = 10^4 \frac{\sum_k (A_{n+1})_k}{\sum_k (B_{m+1})_k}, \tag{1.5.84b}$$

where the summation k is carried over all k blocks with the k^{th} block carrying a current density of J_k and located between radii ρ_{1k} and ρ_{2k} and angles ϕ_{1k} and ϕ_{2k}. The A_n and B_n for each current blocks are computed using the expressions given above. The harmonics are defined such that the fundamental harmonic b_m is normalized to 10^4.

The field components outside a current block ($r > \rho_2$) are obtained similarly by integrating Eqs. (1.5.78) and the results are given below

$$B_r(r,\theta) = -\frac{\mu_o J}{2\pi} \sum_{n=1}^{\infty} \frac{\rho_2^{n+1} - \rho_1^{n+1}}{n(n+2) r^{n+1}} \left[cos(n(\phi_2 - \theta)) - cos(n(\phi_1 - \theta)) \right], \tag{1.5.85a}$$

$$B_\theta(r,\theta) = \frac{\mu_o J}{2\pi} \sum_{n=1}^{\infty} \frac{\rho_2^{n+1} - \rho_1^{n+1}}{n(n+2) r^{n+1}} \left[sin(n(\phi_2 - \theta)) - sin(n(\phi_1 - \theta)) \right]. \tag{1.5.85b}$$

The field inside a current block ($\rho_1 < r < \rho_2$) can be obtained by dividing the current block in two parts (a) from radius ρ_1 to radius r and (b) from radius r to radius ρ_2. Then the superimposition principle can be used to determine the field components with the (a) part evaluated from Eqs. (1.5.78) with ρ_2 replaced by r and the (b) part from Eqs. (1.5.85) with ρ_1 replaced by r.

1.5.3.5. Field Harmonics due to Current Blocks in a Cylindrical Iron Shell

As shown in a previous section (Eqs. (1.5.67) for $r < a$), the expressions for the field component due to current blocks get modified when they are placed inside an iron shell having an iron inner radius of R_f and outer radius of R_a. The harmonic coefficients A_n and B_n are enhanced by :

$$K_n = \left[1 + \frac{\mu - 1}{\mu + 1}\left(\frac{a}{R_f}\right)^{2n}\right] \frac{\left[1 - \left(\frac{R_f}{R_a}\right)^{2n}\right]}{\left[1 - \left(\frac{\mu-1}{\mu+1}\right)^2 \left(\frac{R_f}{R_a}\right)^{2n}\right]},$$

To give

$$A_n^{'} = K_n \times A_n,$$

and

$$B_n^{'} = K_n \times B_n.$$

The harmonics coefficients a_n and b_n given in Eqs. (1.5.84) are modified to :

$$b_n = 10^4 \frac{\sum_k \left(K_{n+1} \ B_{n+1}\right)_k}{\sum_k \left(K_{m+1} \ B_{m+1}\right)_k} \qquad (1.5.86a)$$

$$a_n = 10^4 \frac{\sum_k \left(K_{n+1} \ A_{n+1}\right)_k}{\sum_k \left(K_{m+1} \ B_{m+1}\right)_k} \qquad (1.5.86b)$$

1.5.3.6. COS($m\theta$) Current Distribution for Ideal Fields

In this section, it is demonstrated that an ideal $2m$ (m=1 for dipole) multipolar field shape in accelerator magnets can be produced by a COS($m\theta$) current distribution. In the last section the expressions for the field and vector potential produced by a line current were obtained. The field in the cross section of the magnet can be described by superimposing the field produced by a large number of such wires.

A cylindrical current sheet [12-18] at a radius of a is shown in Fig. 1.5.2, where the angular current density $I(\phi)$ in *Amperes/radian* as a function of angle ϕ is given by the relation

$$I(\phi) \;=\; I_o \;cos(m\phi). \tag{1.5.87}$$

[In the case of skew harmonics the current distribution is $I(\phi) \;=\; I_o \;sin(m\phi)$].

It will be demonstrated that a pure dipole field is created by *m=1*, quadrupole by *m=2*, sextupole by *m=3*, etc. The total current required (Ampere-turns) per pole for generating a $2m$-pole field is given by

$$I_{pole} \;=\; \int_o^{\pi/2m} I_o \;cos(m\phi)\; d\phi \;=\; \frac{I_o}{m}.$$

In Eqs. (1.5.39), the vector potential produced by a single wire at any position is computed. To obtain the vector potential at (r,θ) inside the sheet (i.e. r $< a$), the expression is integrated over ϕ

$$A_z(r,\theta) = \frac{\mu_o I_o}{2\pi}\sum_{n=1}^{\infty}\left(\frac{1}{n}\right)\left(\frac{r}{a}\right)^n \int_o^{2\pi} cos(m\phi)\;\; cos(n(\phi-\theta))\;\; d\phi, \tag{1.5.88}$$

to obtain

$$A_z(r,\theta) = \frac{\mu_o I_o}{2m}\left(\frac{r}{a}\right)^m cos(m\theta), \tag{1.5.89}$$

where the following trigonometric relations have been used

$$cos[n(\phi-\theta)] = cos(n\phi)\;\; cos(n\theta) + sin(n\phi)\;\; sin(n\theta), \tag{1.5.90}$$

$$\int_o^{2\pi} cos(m\phi)\;\; cos(n\phi)\;\; d\phi = \pi\delta_{m,n}, \tag{1.5.91a}$$

$$\int_o^{2\pi} cos(m\phi)\;\; sin(n\phi)\;\; d\phi = 0. \tag{1.5.91b}$$

The field components inside the current sheet are obtained by using Eqs. (1.5.40)

$$B_\theta(r,\theta) = -\frac{\mu_o I_o}{2a}\left(\frac{r}{a}\right)^{m-1} cos(m\theta), \tag{1.5.92a}$$

$$B_r(r,\theta) = -\frac{\mu_o I_o}{2a}\left(\frac{r}{a}\right)^{m-1} sin(m\theta), \tag{1.5.92b}$$

$$B_z(r,\theta) = 0. \tag{1.5.92c}$$

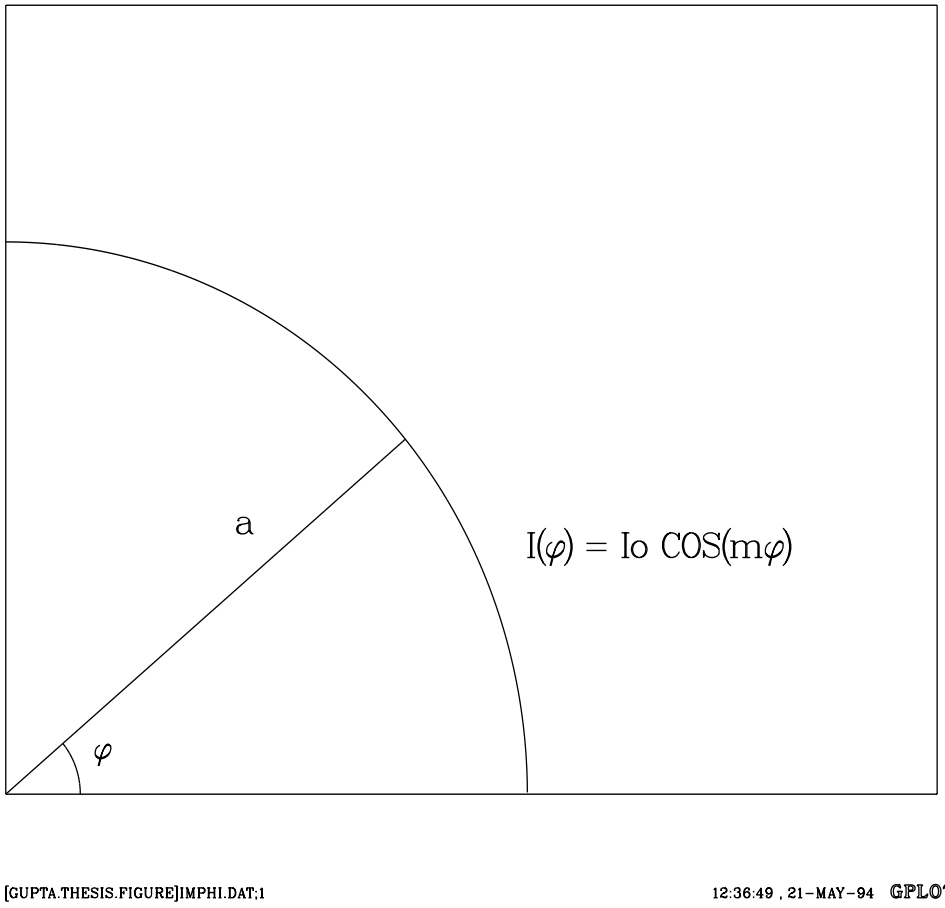

Figure 1.5.2: Computation of the field at (r, θ) produced by a current sheet at a radius a in which the current density varies as a function of angle given by $I(\phi) = I_o \cos(m\phi)$.

It may be noted that the magnitude of the field $|B|$ is independent of θ. On using Eqs. (1.5.46)

$$B_x(r,\theta) = -\frac{\mu_o I_o}{2a}\left(\frac{r}{a}\right)^{m-1} \sin((m-1)\theta), \qquad (1.5.93a)$$

$$B_y(r,\theta) = -\frac{\mu_o I_o}{2a}\left(\frac{r}{a}\right)^{m-1} \cos((m-1)\theta). \qquad (1.5.93b)$$

For the m=1 case, this generates a pure dipole field, as the field components from Eqs. (1.5.92) reduce to

$$B_\theta\,(r,\theta) = -\frac{\mu_o I_o}{2a} cos\,(\theta)\,,$$
$$B_r\,(r,\theta) = -\frac{\mu_o I_o}{2a} sin\,(\theta)\,,$$

and, from Eqs. (1.5.93)

$$B_x = 0, \tag{1.5.94a}$$
$$B_y = -\frac{\mu_o I_o}{2a}. \tag{1.5.94b}$$

This implies that a cylindrical current sheet with a cosine θ current distribution would create a uniform vertical field inside it. This basic result is widely used in designing superconducting accelerator dipole magnets, although the actual current distribution is somewhat modified for practical reasons.

Likewise, for m=2, a pure quadrupole field is generated

$$B_\theta\,(r,\theta) = -\frac{\mu_o I_o r}{2a^2} cos\,(2\theta)\,,$$
$$B_r\,(r,\theta) = -\frac{\mu_o I_o r}{2a^2} sin\,(2\theta)\,,$$

and, from Eqs. (1.5.93)

$$B_x = g\ \ y, \tag{1.5.95a}$$
$$B_y = g\ \ x, \tag{1.5.95b}$$

with $g = -(\mu_o I_o)/(2a^2)$.

Similarly, for m=3, a pure sextupole field is generated

$$B_\theta\,(r,\theta) = -\frac{\mu_o I_o r^2}{2a^3} cos\,(3\theta)\,,$$
$$B_r\,(r,\theta) = -\frac{\mu_o I_o r^2}{2a^3} sin\,(3\theta)\,,$$

and, from Eqs. (1.5.93)

$$B_x = 2S\ \ x\ \ y, \tag{1.5.96a}$$
$$B_y = S\,(x^2 - y^2)\,, \tag{1.5.96b}$$

with $S = -(\mu_o I_o)/(2a^3)$.

In general, a $cos(m\theta)$ current distribution gives a $2m$ order multipole with field components given by Eqs. (1.5.93).

On the x-axis (midplane), $\theta = 0$, these components become

$$B_x(x,0) = 0, \tag{1.5.97a}$$

$$B_y(x,0) = -\frac{\mu_o I_o}{2a}\left(\frac{x}{a}\right)^{m-1}, \tag{1.5.97b}$$

and on the y-axis

$$\begin{aligned} B_x(0,y) &= 0, && for \quad m = 1,3,5,... \\ &= \pm\frac{\mu_o I_o}{2a}\left(\frac{y}{a}\right)^{m-1}, && for \quad m = 2,4,6,... \end{aligned} \tag{1.5.98a}$$

$$\begin{aligned} B_y(0,y) &= \pm\frac{\mu_o I_o}{2a}\left(\frac{y}{a}\right)^{m-1}, && for \quad m = 1,3,5,... \\ &= 0. && for \quad m = 2,4,6,... \end{aligned} \tag{1.5.98b}$$

To obtain the field outside the current sheet (r > a), Eqs. (1.5.44) is integrated using the trigonometric relations given in Eq. (1.5.90)and Eqs. (1.5.91)

$$\begin{aligned} A_z(r,\theta) = &-\frac{\mu_o I_o}{2\pi} ln\left(\frac{r}{a}\right)\int_o^{2\pi} cos(m\phi)\ d\phi \\ &+ \frac{\mu_o I_o}{2\pi}\sum_{n=1}^{\infty}\left(\frac{1}{n}\right)\left(\frac{a}{r}\right)^n \int_o^{2\pi} cos(m\phi)\ cos(n(\phi-\theta))\ d\phi, \end{aligned}$$

$$\text{therefore, } A_z(r,\theta) = \frac{\mu_o I_o}{2m}\left(\frac{a}{r}\right)^m cos(m\theta). \tag{1.5.99}$$

The field components for r > a are obtained using Eqs. (1.5.40)

$$B_\theta(r,\theta) = \frac{\mu_o I_o}{2a}\left(\frac{a}{r}\right)^{m+1} cos(m\theta), \tag{1.5.100a}$$

$$B_r(r,\theta) = -\frac{\mu_o I_o}{2a}\left(\frac{a}{r}\right)^{m+1} sin(m\theta), \tag{1.5.100b}$$

$$B_z(r,\theta) = 0, \tag{1.5.100c}$$

and the (B_x, B_y) components of the field are obtained as :

$$B_x = B_r\ cos(\theta) - B_\theta\ sin(\theta),$$

and

$$B_y = B_r\ sin(\theta) + B_\theta\ cos(\theta),$$

therefore,

$$B_x = -\frac{\mu_o I_o}{2a}\left(\frac{a}{r}\right)^{m+1} sin[(m+1)\theta], \tag{1.5.101a}$$

$$B_y = \frac{\mu_o I_o}{2a}\left(\frac{a}{r}\right)^{m+1} cos[(m+1)\theta]. \tag{1.5.101b}$$

In the case of the dipole (m=1), the field components outside the current sheet, fall as $\frac{1}{r^2}$, and are given by :

$$B_\theta(r,\theta) = \frac{\mu_o I_o a}{2r^2} cos[\theta], \tag{1.5.102a}$$

$$B_r(r,\theta) = -\frac{\mu_o I_o a}{2r^2} sin[\theta], \tag{1.5.102b}$$

$$B_x(r,\theta) = -\frac{\mu_o I_o a}{2r^2} sin[2\theta], \tag{1.5.102c}$$

$$B_y(r,\theta) = \frac{\mu_o I_o a}{2r^2} cos[2\theta]. \tag{1.5.102d}$$

In deriving the above expressions, for simplicity it is assumed that the current is localized in a sheet. However, in accelerator magnets, the current is present between two radii a_1 and a_2. It is assumed that the current density in Amperes/m^2 is given by

$$J(\phi) \;=\; J_o \; cos(m\phi).$$

For a sheet of infitesimal thickness da, J_o is related to the angular current density (I_o) as

$$I_o \;=\; J_o \; a \; da,$$

In this case the expression for the vector potential and field components for r < a are by integrating Eqs. (1.5.39):

$$A_z(r,\theta) = \frac{\mu_o J_o}{2\pi} \sum_{n=1}^{\infty} \left(\frac{r^n}{n}\right) \int_{a_1}^{a_2} \frac{1}{a^n} a \; da \int_o^{2\pi} cos(m\phi) \;\; cos(n(\phi-\theta)) \;\; d\phi,$$

Therefore,

$$A_z(r,\theta) = \frac{\mu_o J_o r^m}{2m} \; cos(m\theta) \int_{a_1}^{a_2} \frac{1}{a^{m-1}} \; da, \tag{1.5.103}$$

$$B_\theta(r,\theta) = -\frac{\mu_o J_o r^{m-1}}{2} \; cos(m\theta) \int_{a_1}^{a_2} \frac{1}{a^{m-1}} \; da, \tag{1.5.104a}$$

$$B_r(r,\theta) = -\frac{\mu_o J_o r^{m-1}}{2} \; sin(m\theta) \int_{a_1}^{a_2} \frac{1}{a^{m-1}} \; da, \tag{1.5.104b}$$

$$B_z(r,\theta) = 0. \tag{1.5.104c}$$

Except for $m = 2$ case (the quadrupole case, for which the expressions are given later), one obtains :

$$A_z(r,\theta) = \frac{\mu_o J_o {a_1}^2}{2m(m-2)} \; cos(m\theta) \left(\frac{r}{a_1}\right)^m \left(1 - \left(\frac{a_1}{a_2}\right)^{m-2}\right), \tag{1.5.105}$$

$$B_\theta(r,\theta) = -\frac{\mu_o J_o a_1}{2(m-2)} \; cos(m\theta) \left(\frac{r}{a_1}\right)^{m-1} \left(1 - \left(\frac{a_1}{a_2}\right)^{m-2}\right), \tag{1.5.106a}$$

$$B_r(r,\theta) = -\frac{\mu_o J_o a_1}{2(m-2)}\ sin(m\theta)\left(\frac{r}{a_1}\right)^{m-1}\left(1-\left(\frac{a_1}{a_2}\right)^{m-2}\right), \quad (1.5.106b)$$

$$B_y(r,\theta) = -\frac{\mu_o J_o a_1}{2(m-2)}\ cos((m-1)\theta)\left(\frac{r}{a_1}\right)^{m-1}\left(1-\left(\frac{a_1}{a_2}\right)^{m-2}\right), \quad (1.5.106c)$$

$$B_x(r,\theta) = -\frac{\mu_o J_o a_1}{2(m-2)}\ sin((m-1)\theta)\left(\frac{r}{a_1}\right)^{m-1}\left(1-\left(\frac{a_1}{a_2}\right)^{m-2}\right). \quad (1.5.106d)$$

In the case of the dipole (m=1), this gives a vertical field

$$B_y = -\mu_o J_o\left(\frac{a_2-a_1}{2}\right) = -\mu_o J_o\left(\frac{\Delta a}{2}\right).$$

For $m = 2$ (quadrupole), the integration of Eqs. (1.5.104) gives :

$$A_z(r,\theta) = \frac{\mu_o J_o r^2}{4}\ cos(2\theta)\ \ ln\left(\frac{a_2}{a_1}\right) \quad (1.5.107)$$

$$B_\theta(r,\theta) = -\frac{\mu_o J_o r}{2}\ cos(2\theta)\ \ ln\left(\frac{a_2}{a_1}\right) \quad (1.5.108a)$$

$$B_r(r,\theta) = -\frac{\mu_o J_o r}{2}\ sin(2\theta)\ \ ln\left(\frac{a_2}{a_1}\right) \quad (1.5.108b)$$

$$B_y(r,\theta) = -\frac{\mu_o J_o r}{2}\ cos(\theta)\ \ ln\left(\frac{a_2}{a_1}\right) \quad (1.5.108c)$$

$$B_x(r,\theta) = -\frac{\mu_o J_o r}{2}\ sin(\theta)\ \ ln\left(\frac{a_2}{a_1}\right) \quad (1.5.108d)$$

If the sheet thickness $\Delta a = a_2 - a_1$ is very small compared to the the average radius $\bar{a} = \frac{(a_2+a_1)}{2}$, then the expressions in Eqs. (1.5.106) for $r < a$ may be simplified to the following equations since the integral in Eq. (1.5.103) and Eqs. (1.5.104) can be approximated as $(\Delta a/\bar{a}^{m-1})$:

$$A_z(r,\theta) = \frac{\mu_o J_o r \Delta a}{2m}\left(\frac{r}{\bar{a}}\right)^{m-1}\ cos(m\theta), \quad (1.5.109)$$

$$B_\theta(r,\theta) = -\frac{\mu_o J_o \Delta a}{2}\left(\frac{r}{\bar{a}}\right)^{m-1}\ cos(m\theta), \quad (1.5.110a)$$

$$B_r(r,\theta) = -\frac{\mu_o J_o \Delta a}{2}\left(\frac{r}{\bar{a}}\right)^{m-1}\ sin(m\theta). \quad (1.5.110b)$$

1.5.3.7. COS($m\theta$) Current Distribution in a Cylindrical Iron Shell

In superconducting accelerator magnets, the coils are frequently placed inside a cylindrical iron yoke to (a) reduce the stray magnetic field outside the magnet and (b) as an added benefit to enhance the field in the aperture of the magnet. Due to the non-linear properties of the iron, the fraction of field generated by the iron at any current depends on how much the yoke is magnetized. This is too complex a problem to solve analytically. However, one can obtain simple expressions if one assumes that the permeability (μ) of the iron is constant everywhere in the yoke. Expressions for the vector potential and the field are given for the case in which a $COS(m\theta)$ current sheet at radius a is inside in an iron shell with inner radius of R_f and outer radius of R_a.

In this case, the method of matching the boundary conditions at the air and iron interfaces, as described in the last section, can be used to include the contribution from the iron. This is equivalent to the method of images when the effect of the iron is replaced by the equivalent image currents.

In the presence of a cylindrical iron yoke, the vector potential and the field components given in Eqs. (1.5.89) and Eqs. (1.5.92), for $r < a$, are modified to

$$A_z(r,\theta) = \frac{\mu_o I_o}{2m}\ cos(m\theta)\left(\frac{r}{a}\right)^m \times \left[1 + \frac{\mu-1}{\mu+1}\left(\frac{a}{R_f}\right)^{2m} \frac{\left[1-\left(\frac{R_f}{R_a}\right)^{2m}\right]}{\left[1-\left(\frac{\mu-1}{\mu+1}\right)^2\left(\frac{R_f}{R_a}\right)^{2m}\right]}\right], \tag{1.5.111}$$

$$B_\theta(r,\theta) = -\frac{\mu_o I_o}{2a}\ cos(m\theta)\left(\frac{r}{a}\right)^{m-1} \times \left[1 + \frac{\mu-1}{\mu+1}\left(\frac{a}{R_f}\right)^{2m} \frac{\left[1-\left(\frac{R_f}{R_a}\right)^{2m}\right]}{\left[1-\left(\frac{\mu-1}{\mu+1}\right)^2\left(\frac{R_f}{R_a}\right)^{2m}\right]}\right], \tag{1.5.112a}$$

$$B_r(r,\theta) = -\frac{\mu_o I_o}{2a}\ sin(m\theta)\left(\frac{r}{a}\right)^{m-1} \times \left[1 + \frac{\mu-1}{\mu+1}\left(\frac{a}{R_f}\right)^{2m} \frac{\left[1-\left(\frac{R_f}{R_a}\right)^{2m}\right]}{\left[1-\left(\frac{\mu-1}{\mu+1}\right)^2\left(\frac{R_f}{R_a}\right)^{2m}\right]}\right]. \tag{1.5.112b}$$

The other components are obtained using Eqs. (1.5.46)

$$B_x(r,\theta) = -\frac{\mu_o I_o}{2a}\ sin((m-1)\theta)\left(\frac{r}{a}\right)^{m-1} \times$$

$$\left[1+\frac{\mu-1}{\mu+1}\left(\frac{a}{R_f}\right)^{2m}\frac{\left[1-\left(\frac{R_f}{R_a}\right)^{2m}\right]}{\left[1-\left(\frac{\mu-1}{\mu+1}\right)^{2}\left(\frac{R_f}{R_a}\right)^{2m}\right]}\right], \qquad (1.5.113a)$$

$$B_y(r,\theta) = -\frac{\mu_o I_o}{2a}\ cos\left((m-1)\theta\right)\left(\frac{r}{a}\right)^{m-1} \times$$

$$\left[1+\frac{\mu-1}{\mu+1}\left(\frac{a}{R_f}\right)^{2m}\frac{\left[1-\left(\frac{R_f}{R_a}\right)^{2m}\right]}{\left[1-\left(\frac{\mu-1}{\mu+1}\right)^{2}\left(\frac{R_f}{R_a}\right)^{2m}\right]}\right], \qquad (1.5.113b)$$

$$B_z(r,\theta) = 0. \qquad (1.5.113c)$$

Similarly, the vector potential and field outside the current sheet but inside the iron, i.e. $a < r < R_f$, is given by :

Between Coil and Iron ($\mathbf{a < r < R_f}$)

$$A_z(r,\theta) = \frac{\mu_o I_o}{2m}\left(1+\frac{\mu-1}{\mu+1}\left(\frac{r}{R_f}\right)^{2m}\frac{\left[1-\left(\frac{R_f}{R_a}\right)^{2m}\right]}{\left[1-\left(\frac{\mu-1}{\mu+1}\right)^{2}\left(\frac{R_f}{R_a}\right)^{2m}\right]}\right) \times$$

$$\left(\frac{a}{r}\right)^{m} cos\left(m\theta\right), \qquad (1.5.114)$$

$$B_r = -\frac{\mu_o I_o}{2a}\left(1+\frac{\mu-1}{\mu+1}\left(\frac{r}{R_f}\right)^{2m}\frac{\left[1-\left(\frac{R_f}{R_a}\right)^{2m}\right]}{\left[1-\left(\frac{\mu-1}{\mu+1}\right)^{2}\left(\frac{R_f}{R_a}\right)^{2m}\right]}\right) \times$$

$$\left(\frac{a}{r}\right)^{m+1} sin\left(m\theta\right), \qquad (1.5.115a)$$

$$B_\theta = \frac{\mu_o I_o}{2a}\left(1-\frac{\mu-1}{\mu+1}\left(\frac{r}{R_f}\right)^{2m}\frac{\left[1-\left(\frac{R_f}{R_a}\right)^{2m}\right]}{\left[1-\left(\frac{\mu-1}{\mu+1}\right)^{2}\left(\frac{R_f}{R_a}\right)^{2m}\right]}\right) \times$$

$$\left(\frac{a}{r}\right)^{m+1} cos\left(m\theta\right). \qquad (1.5.115b)$$

Inside Iron ($\mathbf{R_f < r < R_a}$)

$$A_z(r,\theta) = \frac{\mu\mu_o I_o}{m\left(\mu+1\right)}\left(\frac{1-\frac{\mu-1}{\mu+1}\left(\frac{r}{R_a}\right)^{2m}}{1-\left(\frac{\mu-1}{\mu+1}\right)^{2}\left(\frac{R_f}{R_a}\right)^{2m}}\right) \times$$

$$\left(\frac{a}{r}\right)^{m} cos\left(m\theta\right), \qquad (1.5.116)$$

$$B_r = -\frac{\mu\mu_o I_o}{a\left(\mu+1\right)}\left(\frac{1-\frac{\mu-1}{\mu+1}\left(\frac{r}{R_a}\right)^{2m}}{1-\left(\frac{\mu-1}{\mu+1}\right)^{2}\left(\frac{R_f}{R_a}\right)^{2m}}\right) \times$$

$$\left(\frac{a}{r}\right)^{m+1} sin\left(m\theta\right), \tag{1.5.117a}$$

$$B_\theta = \frac{\mu\mu_o I_o}{a\left(\mu+1\right)} \left(\frac{1+\frac{\mu-1}{\mu+1}\left(\frac{r}{R_a}\right)^{2m}}{1-\left(\frac{\mu-1}{\mu+1}\right)^2\left(\frac{R_f}{R_a}\right)^{2m}}\right) \times$$

$$\left(\frac{a}{r}\right)^{m+1} cos\left(m\theta\right). \tag{1.5.117b}$$

Outside Iron ($\mathbf{r > R_a}$)

$$A_z\left(r,\theta\right) = \frac{2\mu\mu_o I_o}{m\left(\mu+1\right)^2} \frac{1}{1-\left(\frac{\mu-1}{\mu+1}\right)^2\left(\frac{R_f}{R_a}\right)^{2m}} \left(\frac{a}{r}\right)^m cos\left(m\theta\right), \tag{1.5.118}$$

$$B_r = -\frac{2\mu\mu_o I_o}{a\left(\mu+1\right)^2} \frac{1}{1-\left(\frac{\mu-1}{\mu+1}\right)^2\left(\frac{R_f}{R_a}\right)^{2m}} \left(\frac{a}{r}\right)^{m+1} sin\left(m\theta\right), \tag{1.5.119a}$$

$$B_\theta = \frac{2\mu\mu_o I_o}{a\left(\mu+1\right)^2} \frac{1}{1-\left(\frac{\mu-1}{\mu+1}\right)^2\left(\frac{R_f}{R_a}\right)^{2m}} \left(\frac{a}{r}\right)^{m+1} cos\left(m\theta\right). \tag{1.5.119b}$$

1.5.3.8. Intersecting Circles with a Constant Current Density for Ideal Fields

It has been shown [137] that a pure dipole field can be created simply by two intersecting circles carrying constant current densities in opposite directions. To demonstrate this, the field is evaluated inside and outside a circular conductor with a radius a and carrying a constant current density J in the direction of the axis (perpendicular to the plane of paper). For a radius $R > a$ (outside the conductor), Ampere's law gives

$$2\pi R \cdot H = \pi a^2 \ J.$$

Therefore,

$$H = \frac{Ja^2}{2R}. \tag{1.5.120}$$

The direction of the magnetic field is azimuthal, with (x, y) components of the field at any point outside the conductor given by

$$H_x = -\frac{Ja^2}{2R} sin\,(\theta) = -\frac{J}{2}\left(\frac{a}{R}\right)^2 y,$$
$$H_y = \frac{Ja^2}{2R} cos\,(\theta) \quad = \frac{J}{2}\left(\frac{a}{R}\right)^2 x.$$

The field inside the conductor $(R < a)$ can be obtained as

$$2\pi R \cdot H = \pi R^2 \ J,$$
$$i.e., \qquad H = \frac{JR}{2}. \tag{1.5.121}$$

with the components of the field being given by

$$H_x = -\frac{J}{2} R \ sin\,(\theta) = -\frac{J}{2} y,$$
$$H_y = \frac{J}{2} R \ cos\,(\theta) \quad = \frac{J}{2} x.$$

Now expressions will be derived for the field produced by the conductors in two intersecting circles. The coordinate system is defined such that the x-axis passes through the centers of the two circles with the origin of the new coordinate system $(x^{'}, y^{'})$ being in the middle of the two. The distance between the centers of the two circles is s with circle 2 to the right such that $x^{'} = x_1 - \frac{s}{2} = x_2 + \frac{s}{2}$ and $y_1 = y_2 = y^{'}$. The direction of the current is opposite in the two circles, with constant current densities J_1 and $-J_2$ respectively. The components of the field inside the region created by the two intersecting circles can be computed by superimposing the field produced by the conductors in the two circles

$$H_x = \frac{y^{'}}{2}(J_2 - J_1),$$
$$H_y = \frac{x^{'}}{2}(J_1 - J_2) + \frac{s}{4}(J_1 + J_2).$$

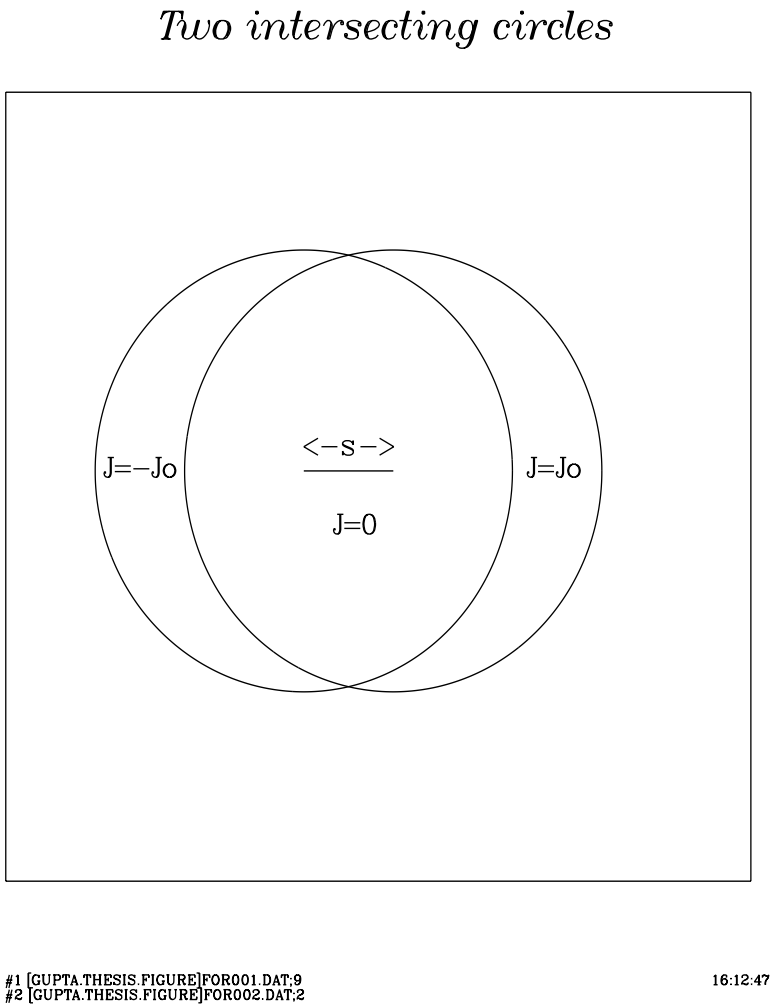

Figure 1.5.3: This figure shows the two intersecting circles of equal size with one carrying a current with a constant density $J = -J_o$ and the other $J = J_o$. The two circles are separated by a distance s. In the intersection region of the two circles, the net current density is zero and therefore it can be replaced by a current free region. It is demonstrated that this configuration produces a vertical dipole field given by $\frac{J_o}{2}s$.

A special case comes when the magnitude of the current densities in the two circles is J_o but the direction is opposite as shown in Fig. 1.5.3. This means that the intersection region is a current free region which can be used as an aperture for the particle beam and and the aperture has a constant vertical magnetic field given by $H_y = \frac{J_o}{2}s$.

It can be shown [14] that four intersecting circles create a quadrupole field and in general $2m$ intersecting circles create a $2m$-order multipole. The treatment has been also been extended to ellipses by a number of authors (see for example Beth [14]).

1.5.4. Complex Variable Method in 2-d Magnetic Field Calculations

The method of complex variable is found very useful in deriving many expressions in superconducting magnets. [12-18,81] These methods can be applied to 2-dimensional field computations, which is the case for the most part of long superconducting magnets. Mills and Morgan [115] have shown that the complex method can also be extended throughout the ends, however, to the field integral ($\int B.dz$). The complex variables have two parts (real and imaginary) and the following variables will be used :

$$z = x \ + \ i \ y, \tag{1.5.122a}$$

$$H(z) = H_y \ + \ i \ H_x, \tag{1.5.122b}$$

$$B(z) = B_y \ + \ i \ B_x, \tag{1.5.122c}$$

$$W(z) = -(A \ + \ i \ \phi) \ + \ constant. \tag{1.5.122d}$$

where W is the complex potential having ϕ and A (scalar and vector potentials) as the two components, and $i \ = \ \sqrt{-1}$. z^* is the complex conjugate of z with

$$z^* = x \ - \ i \ y.$$

In the 2-d case the following relations are valid :

$$B_x = \frac{\partial A}{\partial y} \tag{1.5.123a}$$

$$B_y = -\frac{\partial A}{\partial x}, \tag{1.5.123b}$$

$$with \quad B_x = \mu_0 \mu H_x,$$

$$and \quad B_y = \mu_0 \mu H_y.$$

Moreover, in air ($\mu = 1$),

$$H_x = -\frac{1}{\mu_0}\frac{\partial \phi}{\partial x} = \frac{1}{\mu_0}\frac{\partial A}{\partial y}, \tag{1.5.124a}$$

$$H_y = -\frac{1}{\mu_0}\frac{\partial \phi}{\partial y} = -\frac{1}{\mu_0}\frac{\partial A}{\partial x}. \tag{1.5.124b}$$

The Cauchy-Riemann equations are the necessary and sufficient conditions for a function to be analytic in Z-plane. For a function $F_w \ = \ u \ + \ i \ v$, these conditions are:

$$\frac{\partial u}{\partial x} \ = \ \frac{\partial v}{\partial y}, \tag{1.5.125a}$$

$$\frac{\partial u}{\partial y} \ = -\frac{\partial v}{\partial x}. \tag{1.5.126a}$$

In a medium free of magnetic material with $\mu = 1$, Eqs. (1.5.124) gives

$$\begin{aligned} \frac{\partial A}{\partial x} &= \frac{\partial \phi}{\partial y}, \\ \frac{\partial A}{\partial y} &= -\frac{\partial \phi}{\partial x}, \end{aligned}$$

which are the Cauchy-Riemann conditions for $W(z) = -(A + i\phi) + constant$ to be analytic. In the same way, B(z) (and similarly H(z)) is analytic if :

$$\begin{aligned} \frac{\partial B_y}{\partial x} &= \frac{\partial B_x}{\partial y}, \\ \frac{\partial B_y}{\partial y} &= -\frac{\partial B_x}{\partial x}, \end{aligned}$$

which are just Maxwell's equations in a current free region. It may be noted that the choice of variable $B(z)$ as $B(z) = B_y + iB_x$ is important since B_x and B_y do not the satisfy the Cauchy-Rieman conditions if the variable is $B_x + iB_y$.

Since $W(z)$ is analytic, the derivative of $W(z)$ gives the the complex field function :

$$\frac{dW}{dz} = -\frac{\partial A}{\partial x} - i\ \frac{\partial \phi}{\partial x} = i\ \frac{\partial A}{\partial y} - \frac{\partial \phi}{\partial y} = H_y + i\ H_x = H(z).$$

To deal with a region with current, a new analytic function is defined as follows :

$$F(z) = B(z) - \frac{1}{2}\mu_o J z^* = (B_y - \tfrac{1}{2}\mu_o J x) + i\ (B_x + \tfrac{1}{2}\mu_o J y), \tag{1.5.127}$$

where the current density J is constant throughout the region. The Cauchy-Riemann conditions become :

$$\begin{aligned} & \frac{\partial B_y}{\partial x} - \tfrac{1}{2}\mu_o J = \frac{\partial B_x}{\partial y} + \tfrac{1}{2}\mu_o J \\ \Longrightarrow \quad & \frac{\partial B_y}{\partial x} - \frac{\partial B_x}{\partial y} = \mu_o J \\ & and, \quad \frac{\partial B_y}{\partial y} = -\frac{\partial B_x}{\partial x} \\ \Longrightarrow \quad & \frac{\partial B_x}{\partial x} + \frac{\partial B_y}{\partial y} = 0 \end{aligned}$$

which are Maxwell's equations in the presence of current.

1.5.4.1. Field due to an array of Line Currents

The complex potential at a point z, due a current flowing in a direction perpendicular to the Z-plane at $z = z_o$, is given by :

$$W(z) = \frac{I}{2\pi} \, log(z - z_o) + constant \ ,$$

and the magnetic field is given by :

$$H(z) = \frac{dW}{dz} = \frac{I}{2\pi (z - z_o)}. \tag{1.5.128}$$

The direction of the field is that of $(z - z_o)^*$, which is perpendicular to the vector $(z - z_o)$. The superposition principle can be used to obtain the field due to n filaments with the k^{th} filament carrying I_k amperes and located at $z = z_k$:

$$H(z) = \sum_{k=1}^{n} \frac{I_k}{2\pi (z - z_k)}. \tag{1.5.129}$$

Cauchy's Residue Theorem gives [29]

$$\oint_C f(z) \ dz = 2\pi i \sum_k Res(a_k), \tag{1.5.130}$$

where $Res(a_k)$ are the residues which are defined as the coefficients of $\frac{1}{z - z_k}$ inside the contour C over which the contour integral of the function *f(z)* is taken. Applying this to Eq. (1.5.129) while taking the contour integral of the field around the wires in the Z-plane, one obtains

$$\oint H(z) \ dz = i \sum_{k=1}^{n} I_k. \tag{1.5.131}$$

which is basically Ampere's law.

The Cauchy integral formula [29] gives :

$$f(z_o) = \frac{1}{2\pi i} \oint_C \frac{f(z)}{(z - z_o)} dz, \tag{1.5.132}$$

where the function $f(z)$ is analytic everywhere within and on a closed contour C and $f(z_o)$ is the value of $f(z)$ at $z = z_o$.

1.5.4.2. Beth's Current Sheet Theorem

Beth's *"Current Sheet Theorem"* [12-18] can be derived from Eq. (1.5.131). As shown in Fig. 1.5.4 the current sheet is made up of a number of filaments carrying a total current ΔI perpendicular to the Z-plane along the curve from z to $z + \Delta z$. A contour integral on a closed path enclosing the current sheet will give

$$\oint H(z)\ dz \ = \ i\ \Delta I.$$

Now if the path is squeezed from the right and left sides (indicated by the subscripts R and L) on to the current sheet, then in the limiting case one obtains

$$H_R(z_o) \ - \ H_L(z_o) \ = \ i\ \frac{dI}{dz}, \tag{1.5.133}$$

where $H_R(z_o)$ and $H_L(z_o)$ are the limits of the analytic functions $H_R(z)$ and $H_L(z)$ when z approaches z_o from the right and left and $\frac{dI}{dz}$ is the limit of $\frac{\Delta I}{\Delta z}$ when Δz approaches 0 at any z.

The above equation Eqs. (1.5.133) is called Beth's current sheet theorem. To obtain another equation in potential form this equation is integrated to give

$$W_R(z_o) \ - \ W_L(z_o) \ = \ i\ I \ + \ Constant\ , \tag{1.5.134}$$

where $W_R(z_o)$ and $W_L(z_o)$ are the limits of the analytic functions $W_R(z)$ and $W_L(z)$ when z approaches z_o from the right and left.

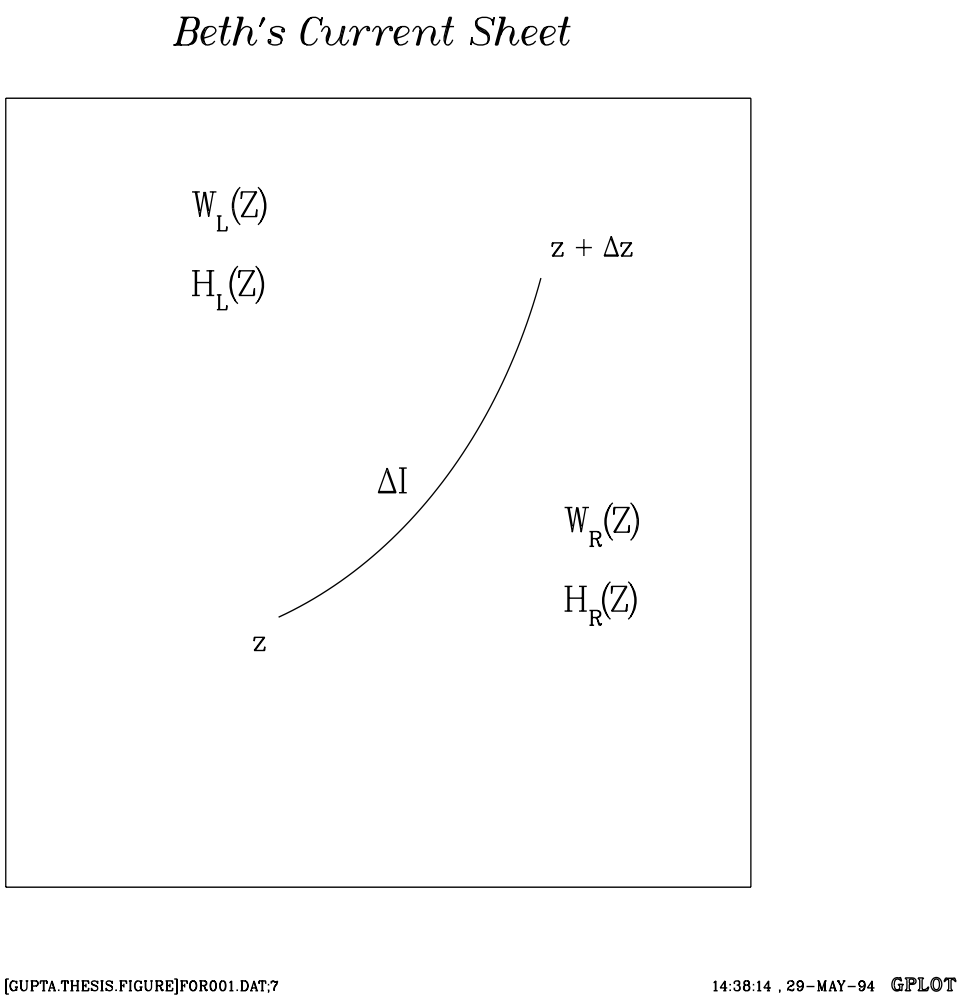

Figure 1.5.4: Beth's current sheet is shown here, which is made up of a number of filaments, carrying a total current ΔI perpendicular to the Z-plane along the curve from z to $z + \Delta z$. The sub-script "R" denotes the right side and "L" denotes the left side to the sheet.

1.5.4.3. Example – Cos(m θ) current distribution

As an example of use of the complex variable methods, expressions are derived here for the field due to a cylindrical current sheet at a radius $r = a$, as shown in Fig. 1.5.2. An angular current density distribution, mentioned earlier, is :

$$\frac{dI}{d\phi} = I_o \cos(m\phi).$$

In complex coordinates, the above current sheet is located at $z = a\ e^{i\phi}$. Then,

$$\frac{dI}{dz} = \left(\frac{dI}{d\phi}\right) / \left(\frac{dz}{d\phi}\right) = \frac{I_o \cos(m\phi)}{i\ a\ e^{i\phi}}.$$

Since H(z) is analytic both inside and outside the current sheet, a general expression for the field to remain finite inside the current sheet ($r < a$) is $H_{in} = \sum_n a_n z^n$ and for outside the current sheet ($r > a$) is $H_{out} = \sum_n b_n z^{-n}$. To obtain the coefficients a_n and b_n, the fields (H_{in}) and (H_{out}) are linked using Beth's current sheet theorem (Eqs. (1.5.133)) as follows :

$$\begin{aligned} H_{out} - H_{in} &= I_o \frac{\cos(m\phi)}{a\ e^{i\phi}} \\ &= \frac{I_o}{2\ a}\left[e^{-i(m+1)\phi} + e^{i(m-1)\phi}\right] \\ &= \frac{I_o}{2\ a}\left[\left(\frac{a}{z}\right)^{m+1} + \left(\frac{z}{a}\right)^{m-1}\right]. \end{aligned}$$

The right hand side of the above equation gives the field on the current sheet and it acts as a boundary condition which must match interior and exterior solutions. Hence a_n=0 for n≠m-1 and b_n=0 for n≠m+1, giving

$$\begin{aligned} H_{in} &= \frac{-I_o}{2\ a}\left(\frac{z}{a}\right)^{m-1} \qquad |z| < a, \\ H_{out} &= \frac{I_o}{2\ a}\left(\frac{a}{z}\right)^{m+1} \qquad |z| > a. \end{aligned}$$

1.6. Methods Investigated for Improving Field Quality

This section gives a brief summary of the research and development work performed during the course of this work for improving the field quality in superconducting magnets. The work is presented in more detail in chapters 2 through 6. The two major components of the magnet which influence the field quality are the coil and yoke designs. A major effort has been made to develop and apply various methods of obtaining the field quality required in large particle accelerators. The field quality is further improved by using tuning shims for correcting errors after construction. Improvements in the techniques used to analyze the magnets have also been made. In the end, optimized designs for the cross section of the SSC collider dipole and RHIC insertion quadrupole magnet are described. The research work is divided into five chapters. The following is a brief description of each chapter.

1.6.1. Improvements in the Computational and Analysis Methods

A technique has been developed for a computer-aided mechanical measurement of the cross section. This can be used to study the geometry of the coil and iron cross section in an actual magnet as built. It can be used to understand the magnetic performance of a design and also to examine the mechanical deformation in a magnet resulting from the large mechanical forces applied during the magnet assembly. This technique is described in chapter 2.

The computer code POISSON has been extensively used to carry out the calculations presented during the course of this work. In order to make a precise computer model of a magnet and in order to obtain the desired accuracy, this program has been extensively modified. A significant effort has been made developing the techniques used in setting up the mesh which describes the problem, to a desired accuracy. These improvements are also described in chapter 2.

1.6.2. Field Quality Improvements through Yoke Design

An iron yoke is used in superconducting magnets to reduce the fringe field outside the physical boundary of the magnet. In addition, the magnetized yoke iron also contributes to the field at the center of the magnet. However, the magnetization is not proportional (linear) to the current in the coil. This contribution becomes non-linear when the field in the iron is above ~1.2 Tesla. This non-linearity in iron properties (referred to commonly as saturation effects) complicates the design and limits the field quality of the magnet at high field. The iron saturation changes the azimuthal distribution of the yoke magnetization. This in turn changes the uniformity of the field in the magnet aperture.

In the magnet designs described in this research work, the saturation effects are minimized by controlling the iron saturation across the azimuth. The path of the magnetic field lines is controlled with the help of a number of techniques so that the iron saturates uniformly throughout the yoke.

The field in the accelerator magnets is represented by the harmonic components and they change with the azimuthal distribution of the field. In an ideal magnet all except one harmonic is zero. In RHIC dipole magnets these yoke design techniques have resulted in reducing the saturation induced harmonics by about an order of magnitude. These involve (a) optimizing the locations of certain holes in the yoke which must be there, or (b) putting in some additional holes which are dedicated to controlling the saturation or (c) putting in cutouts or bumps to shape the aperture or (d) using a non-circular aperture having multiple circular arcs with different radii. The field quality improvements obtained through the yoke designs are described in chapter 3.

1.6.3. Field Quality Improvements through Coil Design

For a variety of reasons a significant difference is observed between the design and measured values of harmonics in the magnets. Moreover, sometimes, there are also differences between the component dimensions as used in the original design computations and the component dimensions as delivered for use in the magnets. A systematic study of this is made in chapter 4. To handle such errors the coil cross section is generally iterated. This is also studied in chapter 4. This approach, however, requires a long time to incorporate in the next design of the magnet and is relatively inflexible. In the RHIC interaction region quadrupole magnets, the cross section iterations are accomplished by changing the size of

the midplane shims (thin material at the coil midplane) and the size of the pole shims (thin material at the coil pole). The major advantage of this approach is the fast turn-around time and an ability to iterate the cross section after the coils are made.

An adjustment in the midplane gap has been used in the industry-built 80 mm aperture RHIC arc dipole magnet to minimize the critical b_4 harmonic. This is also described in chapter 4.

An ideal dipole cross section has 2-fold symmetry and an ideal quadrupole has 4-fold symmetry. The RHIC arc and insertion quadrupoles are collared like dipoles to save cost and for design simplicity reasons. This, however, breaks the ideal 4-fold symmetry in the quadrupoles. Earlier RHIC quadrupoles thus built had large undesired harmonics. The harmonics have been compensated in the present design using a method described in chapter 4. This basically involves creating another deliberate asymmetry between the horizontal and vertical planes by making the gap between the two coils asymmetric at the midplane.

1.6.4. Field Quality Improvements after Construction

The ultimate luminosity performance of RHIC is determined by the field quality in the 130 mm aperture interaction region quadrupoles. To overcome the limitations in obtaining a good field quality due to practical manufacturing and assembling tolerances, the method of *Tuning Shims* has been developed. This is described in detail in chapter 5. The method is referred to as the *Tuning Shim Method* because it corrects the measured harmonics in an individual magnet by adjusting the strength of harmonics generated by each of several tuning shims.

The basic principle is as follows : when a magnetic material (shim) is placed inside the yoke aperture, it becomes magnetized and changes the shape of the field at the center of the magnet. This change can be expressed in terms of harmonic components. By properly choosing the location and size of these magnetic shims one can cancel out as many measured harmonics as the number of shims. In the 130 mm aperture RHIC interaction region quadrupoles, the number of tuning shims is eight. They are used to compensate eight critical harmonics. Calculations will be compared with measurements.

In addition to the above method, which corrects the harmonics in the body of the magnet, an integral correction can also be made in the two ends of the magnet. This

scheme was examined for correcting the top-bottom asymmetry in the SSC collider dipole magnets. This is also described in chapter 5.

1.6.5. Optimized Cross section Designs

The ultimate purpose of the above research and development in the design and analysis methods is to obtain optimized cross section designs which produce the required good field quality in superconducting accelerator magnets. A detailed description of the magnetic design of the cross section of the prototype of the 50 mm aperture SSC collider dipole magnets and the 130 mm aperture RHIC insertion quadrupole magnets is given in chapter 6. This chapter also describes the design philosophy and other considerations used in developing the final optimized sets of parameters. Moreover, detailed computations of the field harmonics at various currents and computations of other quantities like the maximum expected field at which the magnet would remain superconducting (quench field), etc. are also given.